8.0 CONCLUSIONS

This report provides a detailed characterization of the ground motions that might affect Jackson Lake Dam due to a large earthquake on the Teton fault. These ground motion results are intended as inputs for engineering analyses of the stability of the dam during large earthquakes as part of an overall risk assessment for Jackson Lake Dam. Advances in the understanding of strong ground motions over the past decade have accrued due to the recording of several large earthquakes and research efforts to understand the seismic source, propagation, and site effects that produce and influence recorded ground motions. These efforts have lead to the development of improved methods of estimating and predicting strong ground motions at sites such at Jackson Lake Dam. These new data and approaches highlight the importance of geologic structure, basin geometry and properties, and site response to at-site ground motion estimation.

Large-scale crustal velocity structure and source radiation strongly influence the amplitudes and durations of ground motions at Jackson Lake Dam. Ground motions are synthesized for a variety of magnitudes and source geometries to quantify peak ground motions scaling and variability associated with earthquake rupture scenarios postulated for earthquakes on nearby Teton fault segments. Rupture of the northern Teton fault segment is likely to produce a **M** 6.9 earthquake for a dip of 60° and **M** 7.0 for a dip of 45° (**M** 7.0 is also used for a dip of 35°), based on moment fault area relations of Wells and Coppersmith (1994). Rupture of the northern and southern Teton fault segments in a single fault rupture increases **M** by ~ 0.2-0.3 based on moment fault area relations of Wells and Coppersmith (1994). Rupture of the northern segment for dips of 35° and 45° involves fault rupture directly beneath the dam. Impacts of 3D crustal velocity structure are substantial and much of the strong motion modeling effort was devoted to accounting for the influences of 3D velocity heterogeneity on ground motion amplitudes and durations and evaluating the influence of fault dip uncertainties on ground motion characteristics. Ground motion modeling revealed that source characterization, particularly the assumed dip of the Teton fault, strongly influenced peak ground motions and ground motion durations. Consequently, significant geological and geophysical subtasks were required to estimate ground motions at the dam. These include 1) geologic source characterization of the Teton fault, 2) analyses of seismicity in the region of the Teton fault and Jackson Lake Dam, 3) analyses of the hangingwall crustal velocity structure and seismic response, 4) empirical site response analyses based on

specific foundation conditions and recorded data at Jackson Lake Dam, and 5) development of ground motion results from the Teton fault for Jackson Lake Dam considering the integrated results of the previous tasks. As a final step, these results are portrayed in a simplified probabilistic framework to facilitate their input to Reclamation risk assessments for Jackson Lake Dam. Analyses of data from the Jackson Lake Seismic Network (JLSN) and from site-response instrumentation operated at Jackson Lake Dam between 1996-2002 in conjunction with the JLSN are major inputs of most of these subtasks.

8.1 Teton Fault Slip Rates

For the ground motion analyses, existing data have been used as the basis for defining the source characteristics of the Teton fault in the ground motion modeling and as the basis for estimating the probability of the modeled results. Fault scarps on Quaternary deposits indicate the locations of the most recently active fault traces and show the variations in slip along the length of the fault. Maximum slip rates on the Teton fault appear to be in the range of 2 to 5 mm/yr along sections of the fault that are located to the west and southwest of Jackson Lake. Estimated slip rates decrease significantly to the north along the west shore of Jackson Lake and the late Quaternary extent of the fault appears to terminate just north of Jackson Lake near Steamboat Mountain. Slip rates decrease more gradually south of Jackson Lake and the southern limit of late Quaternary fault ruptures appear to be in the Phillips Canyon area, west of the town of Jackson. The largest uncertainty in characterization of late Quaternary slip rates along the Teton fault is uncertainty in the age(s) of faulted and unfaulted deposits along the fault trace. The limited detail of the existing geomorphic mapping of the Teton fault scarps and deposits along the range front results in at least a factor of 2 uncertainty in slip rate estimates for the fault. These same limitations also mean that the existing data are not sufficient to determine whether the Teton fault is segmented or to define in detail the extent of any individual paleoseismic ruptures which could be used as proxies for slip distribution or extent in ground motion models. Because of the absence of detailed data on fault segmentation for the Teton fault, three alternative fault rupture models are considered. These models consider a range of fault rupture segmentation from a highly segmented fault which ruptures in sections that are typically 20-25 km in length to a full rupture of the entire 60-km long fault. Among these models, mean average recurrence intervals for a large surface-rupturing earthquake, M ~7, on the Teton fault range from about 700 years to about 2000 years. The mean

average recurrence interval for a large surface-rupturing earthquake on the Teton fault from the weighted combined models is about 1180 years.

8.2 Teton Fault Dip

The assumed dip of the seismogenic, late Quaternary Teton fault is a highly significant input to the modeled ground motions at Jackson Lake Dam. Lower fault dips result in stronger radiation of seismic energy due to the closer proximity of the rupture surface beneath the dam, greater excitation of the low-velocity crustal basin on the hangingwall of the fault, and imply potentially larger seismic moment release due to the larger areas of the fault plane within the zone of brittle fault rupture. There is little direct data to constrain the dip of the late Quaternary Teton fault in northern Jackson Hole. Most previous studies have portrayed a fault dip near 60° (see review by Byrd et al., 1994), although Behrendt et al. (1968) suggested a much lower dip. Recent analyses and compilations of data from large normal-faulting earthquakes, including the 1959 Hebgen Lake and 1983 Borah Peak earthquakes, have suggested that there is a marked preference for fault planes associated with these earthquakes to have dips near 45°, but with a significant spread over a range of 30-60° (e.g., Thatcher and Hill, 1991; Collettini and Simpson, 2001). The results of Behrendt et al. (1968), which indicate a possible intrabasin trace of the Teton fault that lies east of the late Quaternary, currently seismogenic trace, are further evidence that the lower bound for the dip range of the presently active trace is greater than about 30°.

The relative paucity of earthquakes that could be associated with the Teton fault at depth do not provide strong constraints on fault dip. Focal mechanism solutions of earthquakes located east of the surface trace of the Teton fault dips have east-dipping nodal planes that dip from 25° to 60°. There are too few earthquakes located east of the Teton fault, with far too limited spatial coverage to provide a strong constraint on fault dip, although the spatial distribution of earthquakes is consistent with dips of < 50°. 2D finite-difference modeling of two microearthquakes in Section 4 suggests that the Teton fault dips 40°-50°. Waveform modeling of more of the earthquakes located east of the Teton fault may provide better constraints on Teton fault dip at depth and 3D basin velocity structure than are currently available. The emergence of a relatively new normal fault several km west of the large-scale Teton fault with a steep dip of 60-70° (Section 2) suggests that the current large-scale Teton fault may be approaching unfavorably low dips for continued normal

faulting. Thus, the only available information specific to the Teton fault argues for a fault dip of 35° to 40°. In lieu of any other specific information about the dip of the Teton fault at depth, a fault dip of 35° is considered the most reasonable estimate for the Teton fault. Ground motions models of the Teton fault used dips of 35°, 45°, and 60° to ascertain the sensitivity of estimated ground motions to fault dip.

8.3 3D Crustal Velocity Structure

The Jackson Lake Seismic Network and Jackson Lake Dam site-response data were necessary to constrain the 3D velocity structure near the Teton fault and the dam to develop realistic ground motion estimates for the dam. These microearthquake data were used to develop a large-scale 3D velocity using P-wave arrival times in a 3D velocity-hypocenter inversion. This 3D velocity model was modified and extended to include S-wave information to reproduce site-response ground motions from three microearthquakes located near the western, northern, and southern limits of the northern Teton fault segment and the large-scale 3D low-velocity basin containing the dam. The low-velocity basin is ~3-4 km deep at its deepest point and its boundaries have large velocity discontinuities relative to the relatively high-velocity basement rocks that surround the low-velocity basin. The 3D low-velocity basin velocity structure was developed using seismic refraction data (Behrendt et al., 1968; Byrd et al., 1994) and modeling of microearthquake ground motions at the dam. It allows full development of basin edge-refracted shear wave and multiple free-surface-bounce-refracted arrivals observed in the site-response recordings at the dam. These various shear-wave arrivals form complex, long-duration wavetrains following the direct shear arrival by 3-5 s, and that persist for 15-20 s, depending on the distance of the dam from the excited margin of the basin along the great circle path to the epicenter. The relatively strong velocity discontinuities between the low basin velocities and the surrounding high velocity medium are required to reproduce strong shear-wave arrivals that follow the direct shear-wave by 3-7 s in the weak ground motions recorded at the dam. 2D viscoelastic finite-difference modeling of microearthquake ground motions and site response investigations were used to construct relationships between P- and S-wave velocities and P- and S-wave quality factors (Qp and Qs, respectively).

The seismogram modeling of microearthquakes in Section 4 showed that 3D velocity-model Green's functions are necessary to simulate ground motions within the LVB, not just to obtain realistic durations, but to include the constructive interference effects of coherent secondary sources, like LVB-edge S waves. Empirical Green's functions may underestimate 1-4 Hz responses because the coherent LVB-edge S-waves are probably not adequately represented by the eight empirical Green's functions used in Section 6. Near-surface ground motion amplitudes may be very large along the western margin of the LVB due to rupture directivity. Thus, material nonlinearity may occur at the LVB edges; nonlinearity may modify LVB-edge S-wave and surface-wave contributions to LVB ground motions. It may be important to conduct 2D P-SV plane-wave experiments using nonlinear finite-difference or finite-element codes to ascertain if near-surface, LVB-edge nonlinearity substantially influences ground motion durations and amplitudes within the LVB.

Since the majority of ground motions used to develop ground motion attenuation relations are from California, it's important to recognize the significant differences between the crustal velocity structure near the Teton fault and typical California crustal velocity structure. Near-surface P-wave velocities are ~6 km/s near the surface adjacent to the Teton fault. In southern California, P-wave velocities of 6 km/s are typically not encountered until depths of 5-10 km (Hauksson and Haase, 1997). High basement velocities extending to near the surface in the vicinity of the Teton fault translates into very large velocity contrasts between the LVB and surrounding basement rocks, particularly along the western half of the LVB. Thus, even though LVB S-wave velocities are similar to California "rock" or NEHRP site B S-wave velocities (> 720 m/s), the JLDW rock site behaves more like California stiff-soil site with S-wave velocities of 300-to-600 m/s, than a California "rock" site. The large velocity contrasts between the LVB and the basement rock makes the LVB a strong collector of radiated seismic energy (Figure 4-7a), which produces unusually long observed durations at the dam (Section 5) and amplification of ground motions within the LVB.

There are significant caveats concerning the 3D velocity model, particularly the large-scale low-velocity basin that contains the dam. First, while the strong velocity contrast between the basin and the surrounding medium reproduce overall amplitude and duration characteristics of

weak ground motions recorded at the dam, these are the only data that constrain this aspect of the velocity model. The total depth of the basin probably has at least 1 km uncertainties and the overall 3D shape and roughness of the bottom of the basin are poorly constrained by the data analyzed to date. The 2D finite-difference modeling suggested that strong correlated-random velocity variations may exist in the basin, but the velocity model used to estimate ground motions at the dam has no randomization of basin velocities. The only randomization was applied to the medium outside the low-velocity basin in the form of vertical velocity oscillations with wavelengths of ~1 km that are strongest in the highest velocity gradient portions of the model outside the low-velocity basin. More sophisticated velocity randomizations (O'Connell, 1999a) of the 3D velocity were not pursued because that would have exceeded the logistical constraints of the investigation. Since the basin strongly influences peak ground motion scaling and durations at the dam, the uncertainty in the 3D crustal velocity model may be a significant source of ground motion estimation uncertainty at the dam.

8.4 Soil Site Response

Weak-motion site response was measured at Jackson Lake Dam using an array of seven broad-band seismometers. Key observations are the presence of substantial long-period amplification and prolonged duration of shaking beyond some transition point located between stations 13+00 and 24+00; minimal long-period amplification at stations 12+00 and less, referenced to a bedrock site on the right abutment; and, high-frequency de-amplification on treated sections of the north embankment referenced to a site just outside of the treated zone.

Strong ground motions at stations 13+00 and greater are expected to behave non-linearly. The observed weak-motion site response must be modified to account for non-linear soil behavior. The observed site response at station 24+00 is consistent with the 2-D and 3-D response of a sedimentary basin, and likely results from the generation of surface waves, converted phases, and interface waves. These effects are not accounted for by 1-D models. However, available computer codes for estimating non-linear soil behavior are based on propagating an incident body wave (typically a horizontally polarized S wave) through a 1-D soil column. In order to permit use of 1-D non-linear soil response computer codes, while preserving the observed 2-D and 3-D effects of prolonged duration and long-period amplification, the weak-motion impulse response is

modified for input to the non-linear soil response codes at a selected reference depth. There is considerable uncertainty in this method because the reduction of the convolved surface motions to a reference depth cannot accurately account for the depth dependency of surface waves and converted phases.

As discussed in section 5-2, we don't know the precise location of the transition in site response observed between stations 13+00 (JLD2) and 24+00 (JLD3-5). Based on drilling and geophysical logging, we would expect the transition to be near 14+00, although this is not certain. Thus engineering analyses for stations at 14+00 or greater should use the JLD3 response, and stations less than 14+00 should use the JLD2 response.

2D synthetic seismogram modeling of the soil response data show that the extended ground motion durations observed at the surface are likely associated with a mixture of refracted S-waves, and horizontally propagating surface and interface waves. For shallow depths of 0 m to 20 m the largest accelerations after the near-vertical incidence S-wave direct and reflected arrivals consist of a mixture of refracted S-waves and broadband Rayleigh wave Airy phases. For the portion of the dam located within 1.5 km of the southern glacial scour and depths of 30 m and larger, the largest accelerations after the near-vertical incidence S-wave direct and reflected arrivals are associated with refracted S-waves. At distances > 1.5 km from the glacial scour boundary, the Stonely wave produces the largest accelerations for depths of 30 m and larger. The influence of soil nonlinearity on the amplitudes of these interface waves is unknown, although the continued existence of the free surface and internal velocity discontinuities during modulus degradation suggests that these phases will persist as soils respond nonlinearly. Since a significant amount of energy is propagating horizontally at depths of up to 50 m, it is necessary to account for this significant seismic energy in 1D vertical-incident SH nonlinear simulations of nonlinear soil effects, since the existing codes do not simulate the production of these observed phases. Consequently, it is necessary to include the extended durations in the 1D nonlinear inputs to account for observed, broadband, strong-amplitude extended soil response durations, as discussed in Section 6.

The 2D synthetic seismograms show that there is a critical distance range from the southern margin of the glacial scour where peak horizontal acceleration responses are likely to be amplified

relative to most of the embankment section of the dam. This amplification is associated with the constructive interference of the scour basin-edge interface waves, particularly the broadband Airy phases, but also the Stonely wave, with the direct, reflected, and basin-edge refracted S-waves. The critical distance of maximum amplification is a function of the sediment velocities, which limited geophysical measurements (Sirles, 1986) show vary vertically and laterally from near the southern glacial scour margin and the borehole located between stations JLD3 and JLD6. There are no geophysical velocity measurements or ground motion recordings between stations JLD2 (modest amplification) and station JLD3 (strong amplification). Although the 2D velocity model does not contain all the complex features of the glacial scour geometry inferred in Section 2, the 2D finite-difference synthetic results indicate that it is likely that amplifications stronger than those measured at stations JLD3 and JL6 probably occur somewhere between stations JLD2 and JLD3 (along the tallest portion of the embankment section of the dam). Due to the lack of sediment S-wave-velocity information between stations JLD2 and JLD3, it is not possible to indicate the position or magnitude of the additional amplification relative to station JLD3. It is important to understand that the amplification responses at JLD3 are unlikely to represent the maximum amplification along the embankment portion of the dam between stations JLD2 and JLD3.

The glacial scour S-wave velocity structure at the dam is very similar to the Valley of Mexico in Mexico City (Bodin et al., 1997), except that low-velocities extend ~20 m deeper at Jackson Lake Dam. In the Valley of Mexico, monochromatic, large-amplitude ground motions have durations of ~250 s for **M** > 6.5 seismic sources located > 200 km from the site (Lomnitz et al., 1999). In contrast, the closest portion of the Teton fault is located ~10 km from Jackson Lake Dam. However, the Valley of Mexico is probably significantly longer and wider than the glacial scour basin at Jackson Lake Dam, although the total extent of the glacial scour basin north of the dam is unknown. Consequently, it is likely that the durations in the central portion of the Valley of Mexico would be somewhat longer than at Jackson Lake Dam because the propagation times from the edges of the very-low-velocity basin to the basin interior would be longer. In contrast, the S-wave soil velocities are slower and thicker than those found in the Marina District of San Francisco, which suffered extensive damage during the **M** 6.9 1989 Loma Prieta earthquake. The earthquake was located about 90 km away, yet the Marina District exhibited amplification and

extended durations associated with shallow basin response (Graves, 1993). In the Marina District, near-surface S-wave velocities are ~200 m/s (Graves, 1993), about twice the S-wave velocities in the soil section of Jackson Lake Dam. Using a 3D basin velocity model, Graves (1993) was able to reproduce long ground motion durations and amplification of aftershocks recorded in the Marina District basin. The lower soil S-wave velocities at Jackson Lake Dam make it likely that ground motion durations at the dam will be at least double those observed in the Marina District.

8.5 Ground Motion Estimation

The viscoelastic 3D finite difference methods of Graves and Day (2003) and P.C. Liu (pers. comm.) were used to calculate ground motions for frequencies < 1 Hz and empirical Green's functions (EGF) extracted from the Jackson Lake Dam site-response array were used to simulate ground motions for frequencies > 1 Hz. Broadband strong ground motions were produced by blending the 3D finite-difference motions with the high-frequency EGF motions over transition frequency band centered at 1 Hz. Viscoelastic 3D finite difference methods are used for forward-modeling ground simulations of single and multiple segment finite-fault rupture of the Teton fault using the method of P.C. Liu (pers. comm). The reciprocity approach of Graves and Wald (2001), updated as per Graves and Day (2003) to provide a realistic approximation for damping, was used to calculate 3D Green's functions for grids of point sources distributed on the six fault segments used to evaluate ground motions associated with earthquakes on the Teton fault.

In theory there is no reason EGF's could not be used to produce broadband ground motions. In practice, ambient background noise precludes using EGF's for frequencies substantially < 1 Hz. A total of eight microearthquake three-component seismograms obtained from site-response stations in the vicinity of Jackson Lake Dam were used to produce EGF's for ground motion simulations corresponding to earthquake ruptures on the northern Teton fault segment. Seven seismograms were obtained from station JLDW, located on the south abutment of the dam. The EGF's earthquakes were selected because of their proximity to the northern segment of the Teton fault. several of the earthquakes conceivably are located on the Teton fault; the uncertainties in fault dip and hypocenter locations precludes definitive assignment of these earthquakes to the Teton fault.

Ground motion estimation efforts focused on developing ground motion estimates for rock conditions on the south abutment and soil responses at 140 m depth below the embankment section of the dam for scenario earthquakes on the northern segment of the Teton fault. A limited number of multi-segment ground motion simulations were used to establish that the southern Teton fault segment increases the duration of ground shaking at the dam by 10-20 s, but does not substantially increase ground motion amplitudes. Consequently, detailed ground motion modeling focused on ground motion associated with earthquakes on the northern Teton fault segment.

A kinematic rupture model is used that mimics the spontaneous dynamic rupture behavior of a self-similar stress distribution model. Self-similar effective stresses (and slip velocities) are generated over the fault with rise times that are inversely proportional to effective stress. The kinematic model used here produces slip models with $1/k^2$ distributions consistent with estimates of earthquake slip distributions (Somerville *et al.*, 1999) and ω^2 displacement spectra in the far-field. Effective stress correlation lengths were increased by 33% relative to the **M** 6.7 Northridge rupture simulations of O'Connell et al. (2001) to be consistent with the empirical relations of Somerville et al. (1999), that indicate that asperity size increases with magnitude. Rupture velocities were allowed to vary over a wide range (between $0.6*\beta$ to $1.05*\beta$) to allow rupture directivity caustics to develop, and to produce variable rupture times. Effective stresses average 30-40 bars, consistent with stress drops typically associated with normal-faulting earthquakes. Rise times average 2-3 s and combined with average slips of 2-3 m, produce average slip velocities on the fault of ~ 1 m/s.

There is no direct evidence to constrain the dip of the northern segment of the Teton fault beyond placing "reasonable limits" of 35° to 60°. Consequently, ground motions were simulated for dips of 35°, 45°, and 60°. Several thousand earthquake rupture simulations were performed for each fault dip to estimate strong motion variability associated with uncertainties in earthquake rupture behavior. Resulting ground motions were sorted by response spectral ordinate, and the parameters listed in Table 8-1, to produce mean and 84 percentile ground motion estimates for each discrete value of fault dip. These results were compared to the empirical relations of Spudich et al. (1999) for strike-slip/normal faulting ground motions. A significant caveat is that there are NO strong motion recordings of **M** > 6 normal-faulting earthquakes for a hanging wall site located < 12 km

from the fault in a low-velocity basin. The "empirical relations" of Spudich et al. (1999) use reduced amplitude strike-slip data as a proxy for nonexistent normal faulting data.

A number of ground motion quantities are reported for mean and 84% results, including peak velocity, Arias Intensity, and cumulative kinetic energy. Two durations are reported both defined by the duration of motion from the 5% quantile to the 95% quantile of either Arias Intensity or cumulative kinetic energy. The ground motions from the 35° dip scenario (Table 8-1) have the largest peak motions and longest durations because this fault configuration produces the maximum fault area and the largest fault area beneath the dam. Also, the fault is closest to the dam for a dip of 35°. The peak velocities are very large reflecting a significant amount of rupture directivity compounded by the amplifying responses of the large, low-velocity basin.

Table 8-1: Ground Motion Parameters for a 35°-Dipping Northern Teton Fault Segment.

Component	Peak velocity	Arias Intensity	Cumulative energy	Arias duration	Energy duration
	(cm/s)	(m/s)	(J)	(s)	(s)
Downstream mean	146	6.2	10,928	15.1	21.2
Downstream 84%	201	9.3	15,343	17.7	27.9
Cross canyon mean	102	3.5	9,111	18.5	21.2
Cross canyon 84%	135	5.1	14,154	21.4	26.3
Vertical mean	125	2.4	11,233	16.5	14.3
Vertical 84%	147	3.4	15,709	20.1	16.9

Corresponding mean and 84% acceleration response spectra for JLDW are shown in Figures 8-1 and 8-2, respectively. The synthesized ground motions are much more similar to the Spudich et al. (1999) soil responses than the rock responses (Figures 8-1 and 8-2), both in terms of period content and amplitude. The synthesized ground motions have much stronger responses for periods > ~1.5 s than the empirical predictions, consistent with the first-order influences of the large, low-velocity basin on "rock" ground motions at the dam. Similarly, the synthesized shortest period motions (< 0.4 s) are somewhat lower than SEA99 soil responses, because even the rock conditions at Jackson Lake Dam attenuate higher frequencies more strongly than typical

California soil sites.   Corresponding results for dips of 45° and 60° are shown in Tables 8-2 and 8-3.

Of particular note is that mean peak velocities exceed 90 cm/s for all dip scenarios. Mean 45°-dip response spectra are closer to SEA99 soil results than rock results (Figure 8-3), but 84% 45°-dip response spectra (Figure 8-4) and both mean and 84% 60°-dip response spectra (Figures 8-5 and 8-6) have amplitudes more similar to SEA99 rock results, than SEA99 soil results.

Table 8-2: Ground Motion Parameters for a 45°-Dipping Northern Teton Fault Segment.

Component	Peak velocity	Arias Intensity	Cumulative energy	Arias duration	Energy duration
	(cm/s)	(m/s)	(J)	(s)	(s)
Downstream mean	133	4.8	11,767	16.1	23.4
Downstream 84%	171	7.1	16,956	18.1	33.1
Cross canyon mean	111	4.0	10,063	18.5	21.8
Cross canyon 84%	155	6.1	16,010	21.1	27.4
Vertical mean	105	2.4	9,605	16.3	16.7
Vertical 84%	130	3.6	14,111	19.1	20.1

Table 8-3: Ground Motion Parameters for a 60°-Dipping Northern Teton Fault Segment.

Component	Peak velocity	Arias Intensity	Cumulative energy	Arias duration	Energy duration
	(cm/s)	(m/s)	(J)	(s)	(s)
Downstream mean	96	2.7	9,366	18.3	24.8
Downstream 84%	122	3.9	14,100	23.0	33.8
Cross canyon mean	84	2.6	5,616	19.5	26.0
Cross canyon 84%	116	3.9	8,510	22.4	36.0
Vertical mean	76	1.8	4,819	15.9	20.0
Vertical 84%	98	2.6	,7220	18.7	28.2

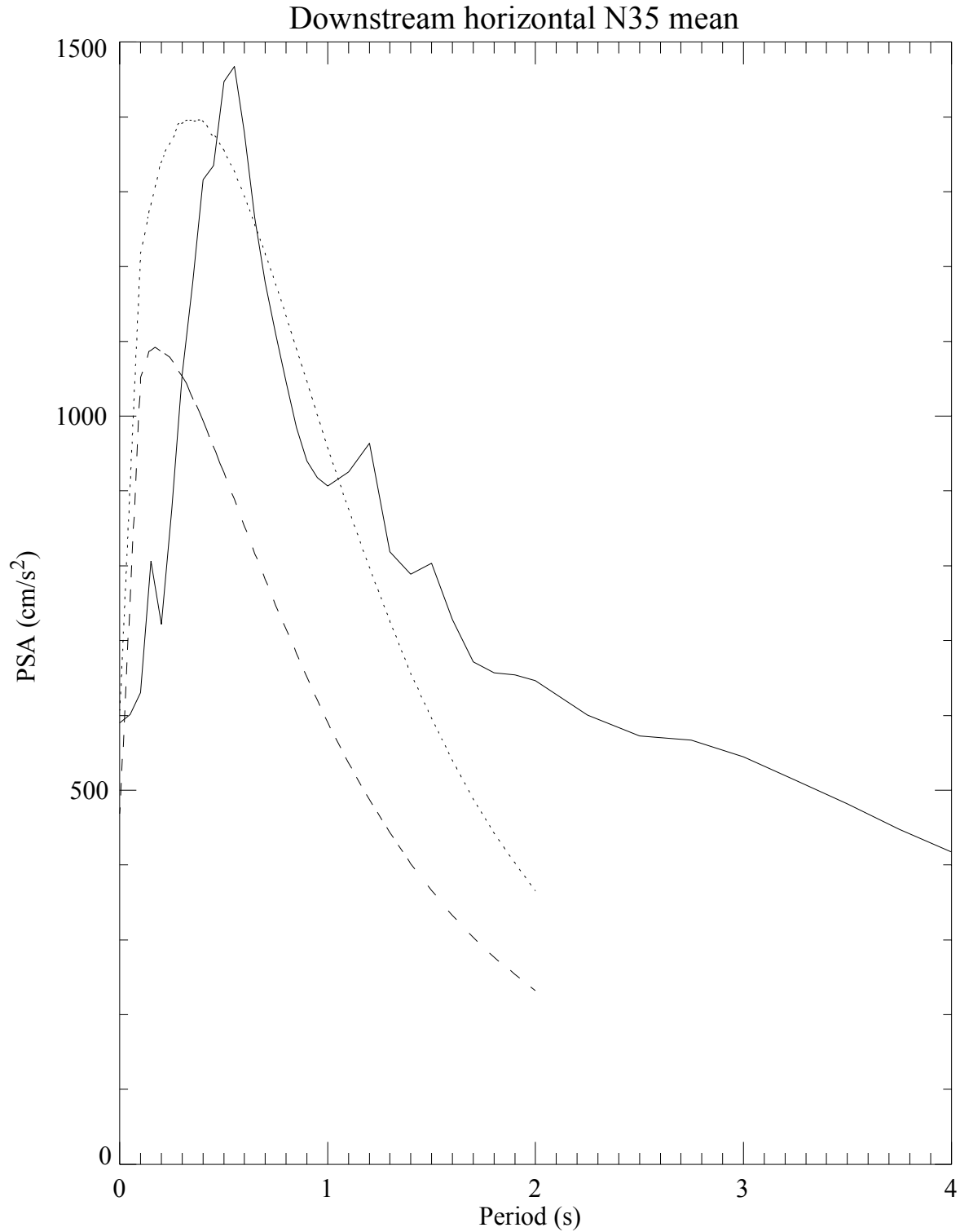## Downstream horizontal N35 mean

Figure 8-1: Mean downstream horizontal JLDW rock site PSA response spectra for a 35°-dipping northern Teton fault segment (solid). Mean Spudich et al. (1999) (SEA99) average horizontal component estimates for a **M** 7.0 normal-faulting earthquake are shown for soil (dotted) and rock (dashed) site conditions.
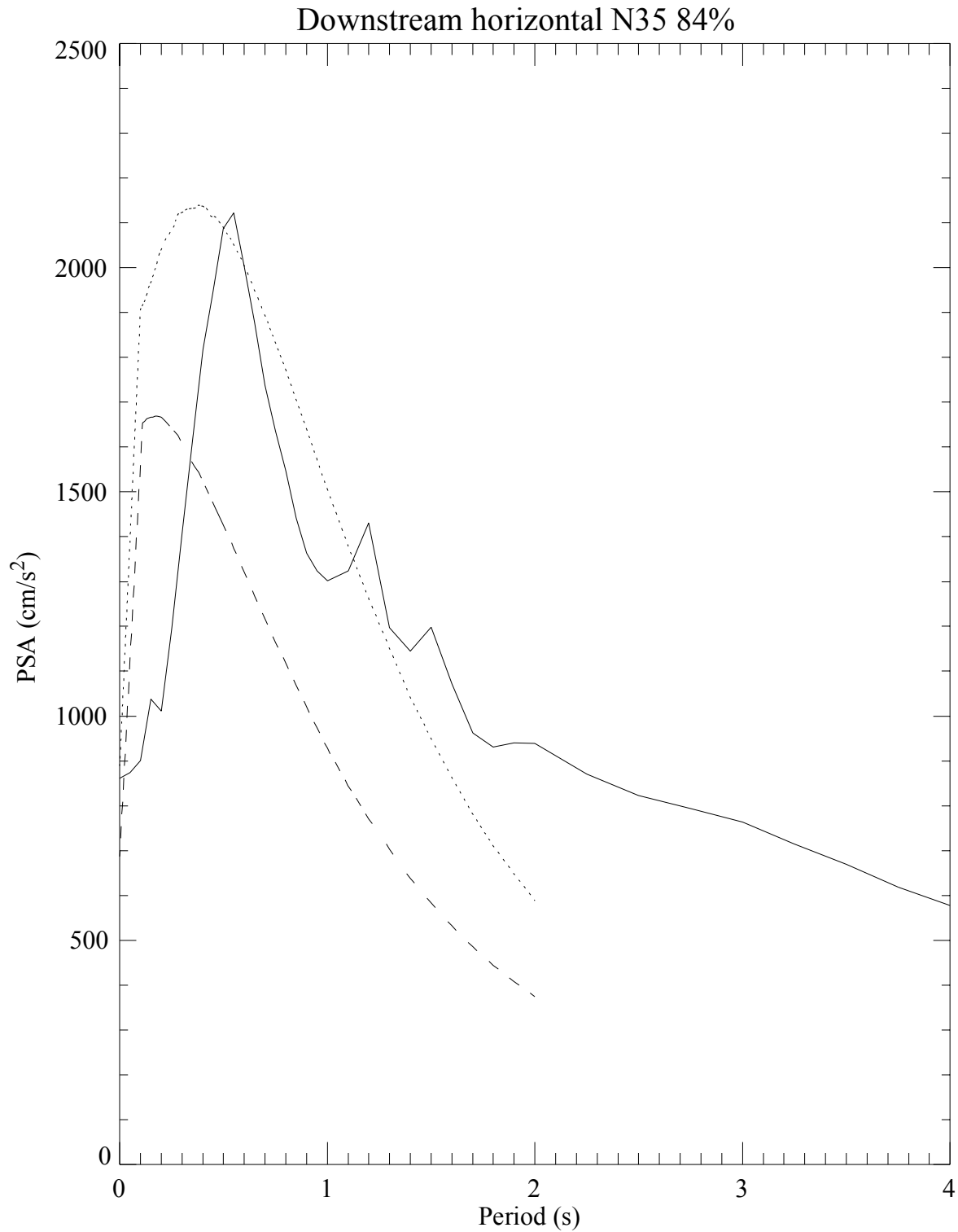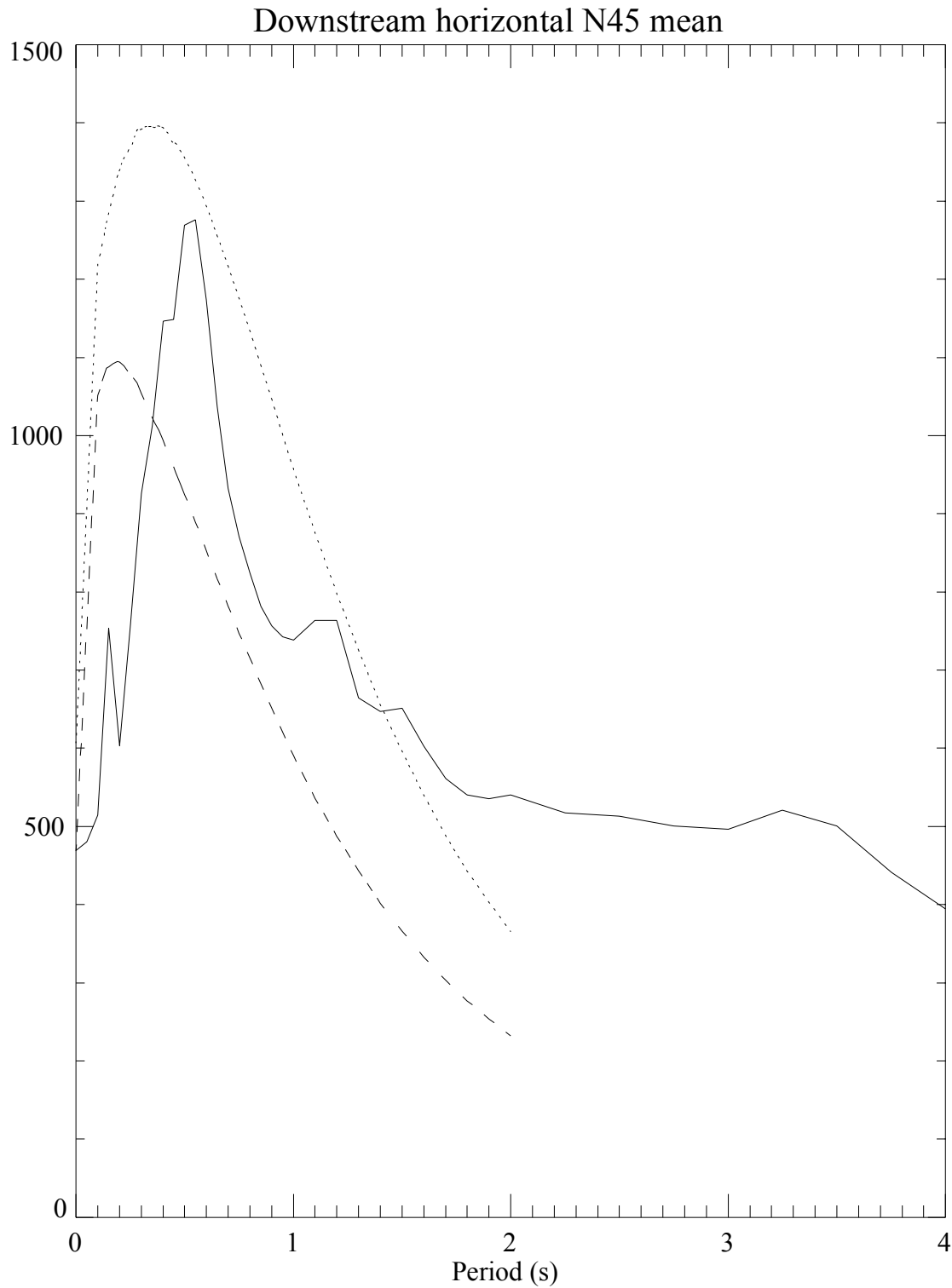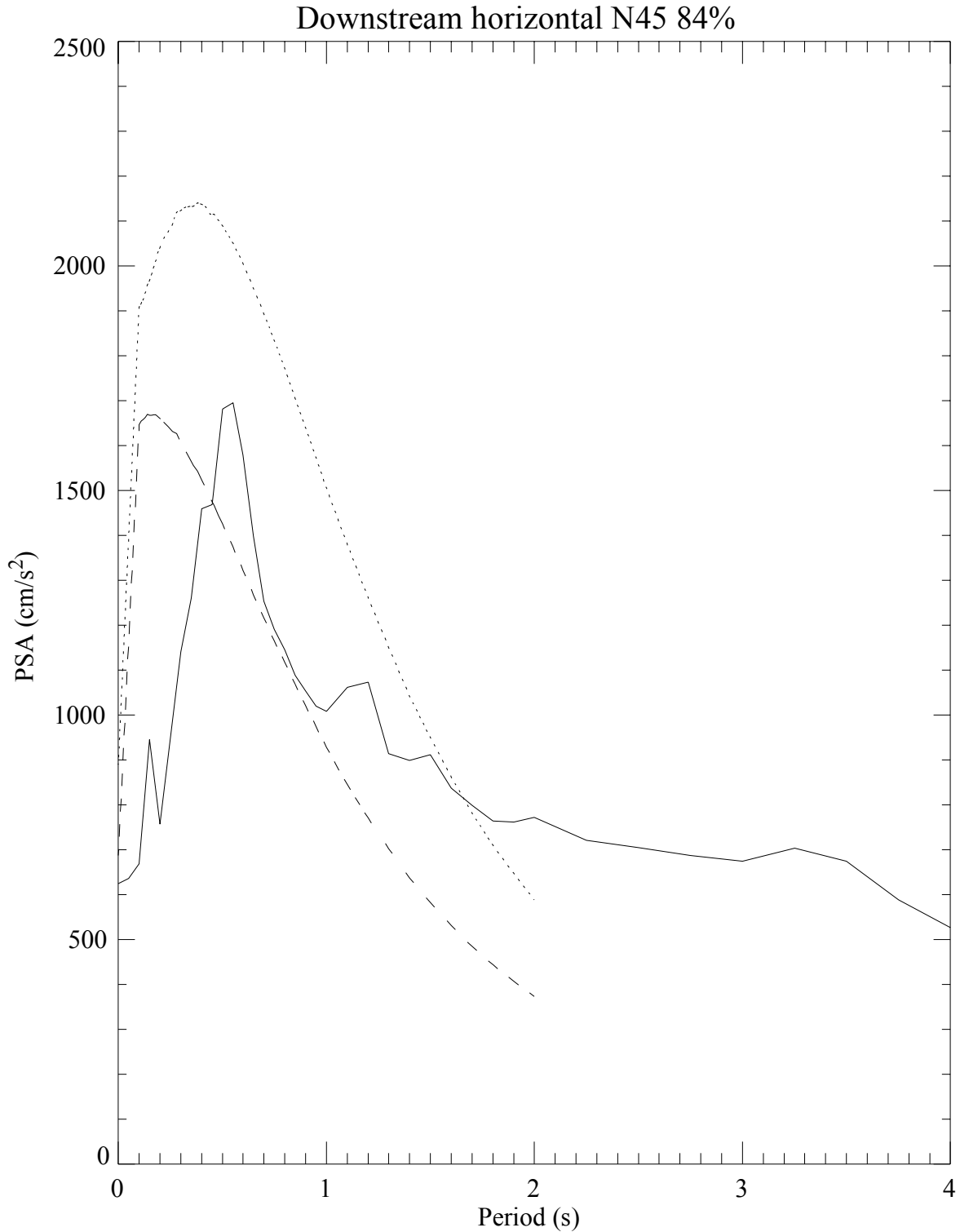
Downstream horizontal N35 84%

Figure 8-2: 84% quantile downstream horizontal JLDW rock site PSA response spectra for a 35°-dipping northern Teton fault segment (solid). 84% SEA99 average horizontal component estimates for a **M** 7.0 normal-faulting earthquake are shown for soil (dotted) and rock (dashed) site conditions.
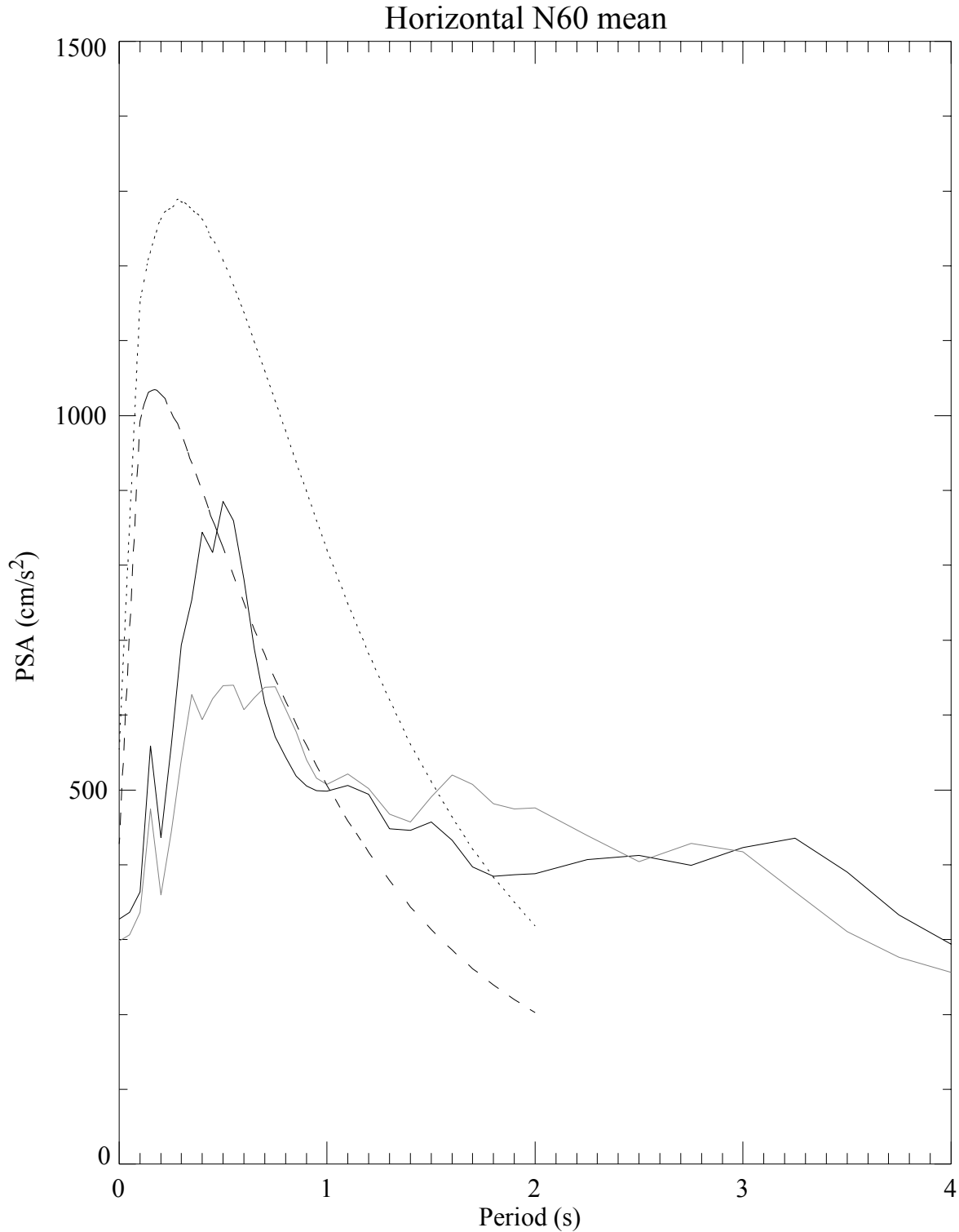
Downstream horizontal N45 mean

Figure 8-3: Mean downstream horizontal JLDW rock site PSA response spectra for a 45°-dipping northern Teton fault segment (solid). Mean SEA99 average horizontal component estimates for a **M** 7.0 normal-faulting earthquake are shown for soil (dotted) and rock (dashed) site conditions.
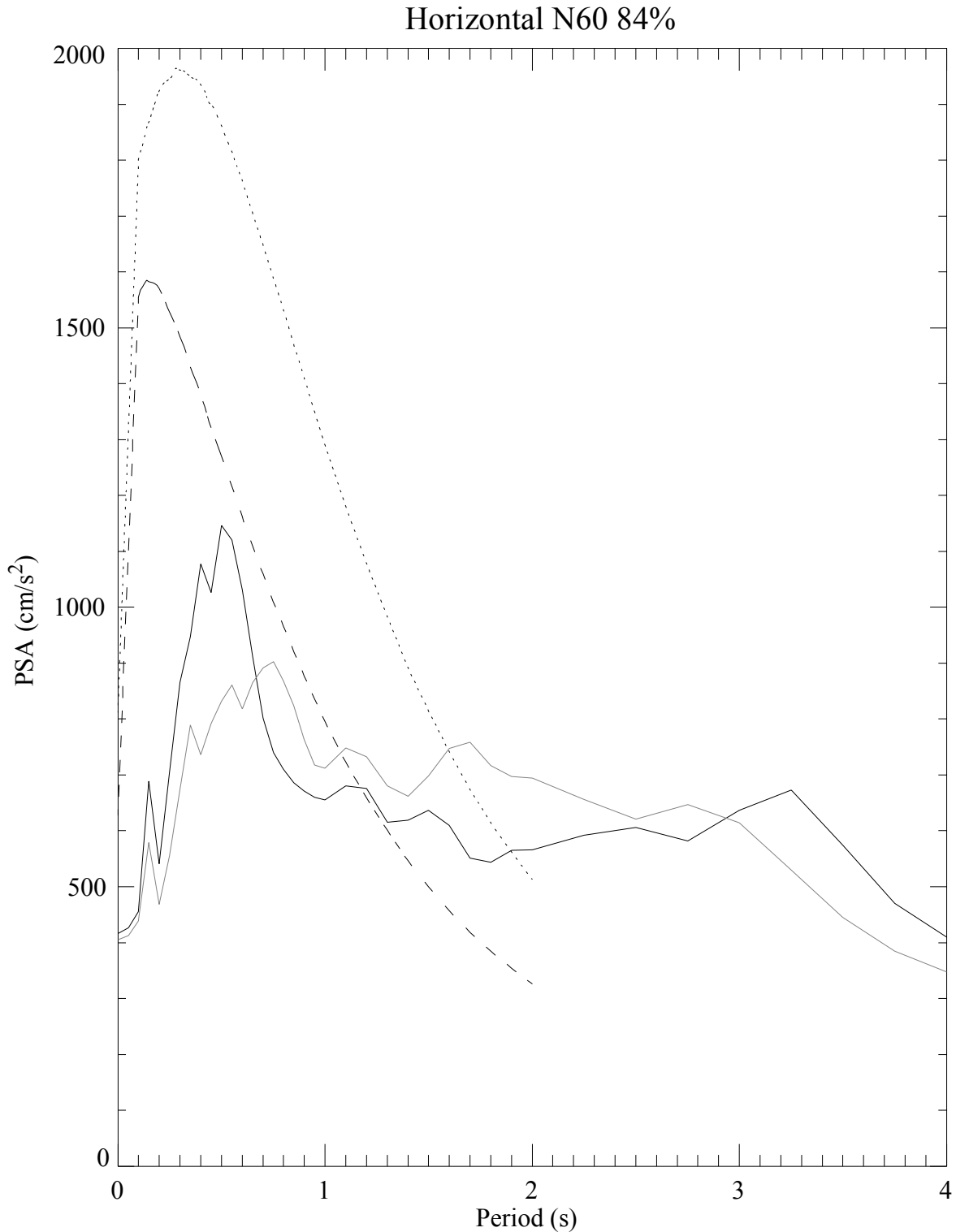
Downstream horizontal N45 84%

Figure 8-4: 84% quantile downstream horizontal JLDW rock site PSA response spectra for a 45°-dipping northern Teton fault segment (solid).   84% SEA99 average horizontal component estimates for a **M** 7.0 normal-faulting earthquake are shown for soil (dotted) and rock (dashed) site conditions.

Horizontal N60 mean

Figure 8-5: Mean JLDW rock site PSA horizontal response spectra for a 60°-dipping northern Teton fault segment.   Downstream is solid and cross canyon is gray. Mean SEA99 average horizontal component estimates for a **M** 6.9 normal-faulting earthquake are shown for soil (dotted) and rock (dashed) site conditions.

Horizontal N60 84%

Figure 8-6: 84% quantile JLDW rock site PSA horizontal response spectra for a 60°-dipping northern Teton fault segment.   Downstream is solid and cross canyon is gray. 84% SEA99 average horizontal component estimates for a **M** 6.9 normal-faulting earthquake are shown for soil (dotted) and rock (dashed) site conditions.

The ground motion simulation approach used in Section 6 was critically evaluated by using alternative ground motion estimation procedures and by confirming that the kinematic rupture model reproduces near-source ground motions from the **M** 6.7 1994 Northridge earthquake. Near-source ground motions from the **M** 6.5 1979 Imperial Valley earthquake are consistent with unusually large long-period acceleration responses predicted for Jackson Lake Dam. The > 0.4 g > 2 s period acceleration responses observed at stations in the low-velocity basin in Imperial Valley indicate that the large (> 0.5 g) > 2 s period acceleration responses predicted for Jackson Lake Dam are not without precedent. Considering the more extreme impedance contrast between the low-velocity sediments and the basement at Jackson Lake Dam relative to Imperial Valley, the large (> 0.5 g) > 2-s-period acceleration responses predicted for Jackson Lake Dam make physical sense, particularly with respect to the incidence angle criteria of Somerville et al. (2003) for predicting the amplification of long-period motions in low-velocity basin. Broadband empirical Green's function investigations in Section 7 confirmed that unusually large accelerations are likely to occur at the dam for periods > 1 s on the horizontal components and for periods extending to 2 s on the vertical component. The broadband EGF ground motions revealed a double parasitic resonance (both the soil and the low-velocity basin are resonating at the same period) for the embankment portion of the dam for periods of 1-2 s for seismic energy arriving from north of the dam. This double resonance strongly amplifies the soil accelerations for periods > 1 s and increases the duration of strong ground shaking to several minutes.

Since the peak ground motions are strongly dependent on the assumed dip of the Teton fault, it is necessary to decide which dip scenario is most representative of expected ground motions at the dam. As discussed in Section 2, worldwide **M** > 5.5 earthquake data for normal-faulting earthquakes indicate that normal-fault dips of ≤ 50° comprise 76% of the normal-faulting earthquakes (Collettini and Sibson, 2001). The focal mechanism data in Section 3 allow for a Teton fault dip of 25° to 60°, but do not place strong constraints on fault dip. As discussed in Section 4, detailed waveform modeling of two earthquakes suggest that the northern Teton fault segment dips < 50°. The local and region evidence for normal-faulting dip suggests that the 35° and 45° fault dip ground motion scenarios represent the most likely dip scenarios for the Teton fault. In view of the lack of any definitive information indicating that the northern Teton fault rupture segment dips > 50°, the 60° fault dip ground motion scenarios are discounted for the

purposes of recommending ground motions for dynamic analyses of Jackson Lake Dam. Although a fault dip of 45° is plausible, the ground motions produced using a fault dip of 35° are recommended for dynamic analyses of Jackson Lake Dam. Our judgement is that the 35°-dipping ground motions are probably most representative of expected ground motions for faults dips < 50°, the most likely range of dips for the Teton fault, based on world-wide distributions of normal fault dips (Section 2) and the limited inferences that can be made about Teton fault dip from microearthquake data (Sections 3 and 4).

8.6 Rock Ground Motions for the Concrete Section

One of the probabilistic parameters requested for use in simplified engineering analyses of the concrete section of Jackson Lake Dam was peak horizontal acceleration (PHA). Since the random seismicity did not significantly contribute to PHA exceeding 0.5 g (see Section 3 and Wong et al., 1999), only ground motions associated with the Teton fault were considered. Specifically, the mean return period for large Teton fault earthquakes of 1180 years from Section 2 was used and the median PHA (0.5 g) and 84% PHA (0.8 g) from Section 6 used to define the annual probabilities. Two different ranges of PHA were of interest for analyses related to the concrete section of the dam. The annual probabilities of PHA within specific requested ranges are provided in Tables 8-4 and 8-5. It must be emphasized that PHA is the least robust and most uncertain of all

Table 8-4: Rock PHA for the Concrete Section, PHA Range 1.

PHA interval	Annual Probability
0.2 - 0.5 g	1/2360
0.5 – 0.8 g	1/3930
> 0.8 g	1/5900

the ground motion quantities estimated for Jackson Lake Dam. There is potential for nonlinearity in the till to modify PHA. In contrast, peak velocities are little affected by nonlinear soil responses

and are robust even with substantial uncertainties in rock and soil properties. The estimates in Tables 8-4 and 8-5 are solely intended for analyses of structures on the rock section of the dam.

Table 8-5: Rock PHA for the Concrete Section, PHA Range 2.

PHA interval	Annual Probability
0.2 - 0.65 g	1/1735
0.65 – 0.8 g	1/9830
> 0.8 g	1/5900

8.7 Rock Ground Motion Time Histories

Synthetic ground motion time histories that were closest to the mean (Figures 8-7 to 8-10) and 84% quantile (Figures 8-11 to 8-14) response spectra were selected to represent mean and 84% ground motions for dynamic analyses of structures on rock. A ground motion from the **M** 7.9 March 13, 1985 Valpariso, Chile earthquake (Figures 8-15 to 8-18) was also recommended to provide sufficiently long shaking durations to correspond to multi-segment rupture of the Teton fault. While this record contains substantial peak acceleration (> 0.8 g), it has relatively small peak velocities compared to the synthetic records. It is recommended that this record be revised to remove some of the response for frequencies > 2 Hz, to produce high-frequency responses more consistent with the synthesized rock site responses in Figure 8-18.

The durations of the mean and 84% synthetic ground motions are lower bounds because the EGFs were limited to durations of 13.5 s after the direct shear-wave arrival. Also, the relatively deterministic nature of the 3D velocity model lacks correlated-random velocity variations that exist in the crust. Consequently, the synthetic low-frequency portions of the motions are also likely to be lower bounds on total ground motion durations. Multi-segment rupture on the Teton fault will likely produce ground motions with 10-15 s longer > ~0.2 g durations that the motions provided in Figures 8-7 to 8-14; this was the motivation for providing the Lleleo record.

The return periods assigned to the individual ground motion time histories reflect multiple sources of uncertainty and natural variability. The average return period for **M** ~6.9-7.1
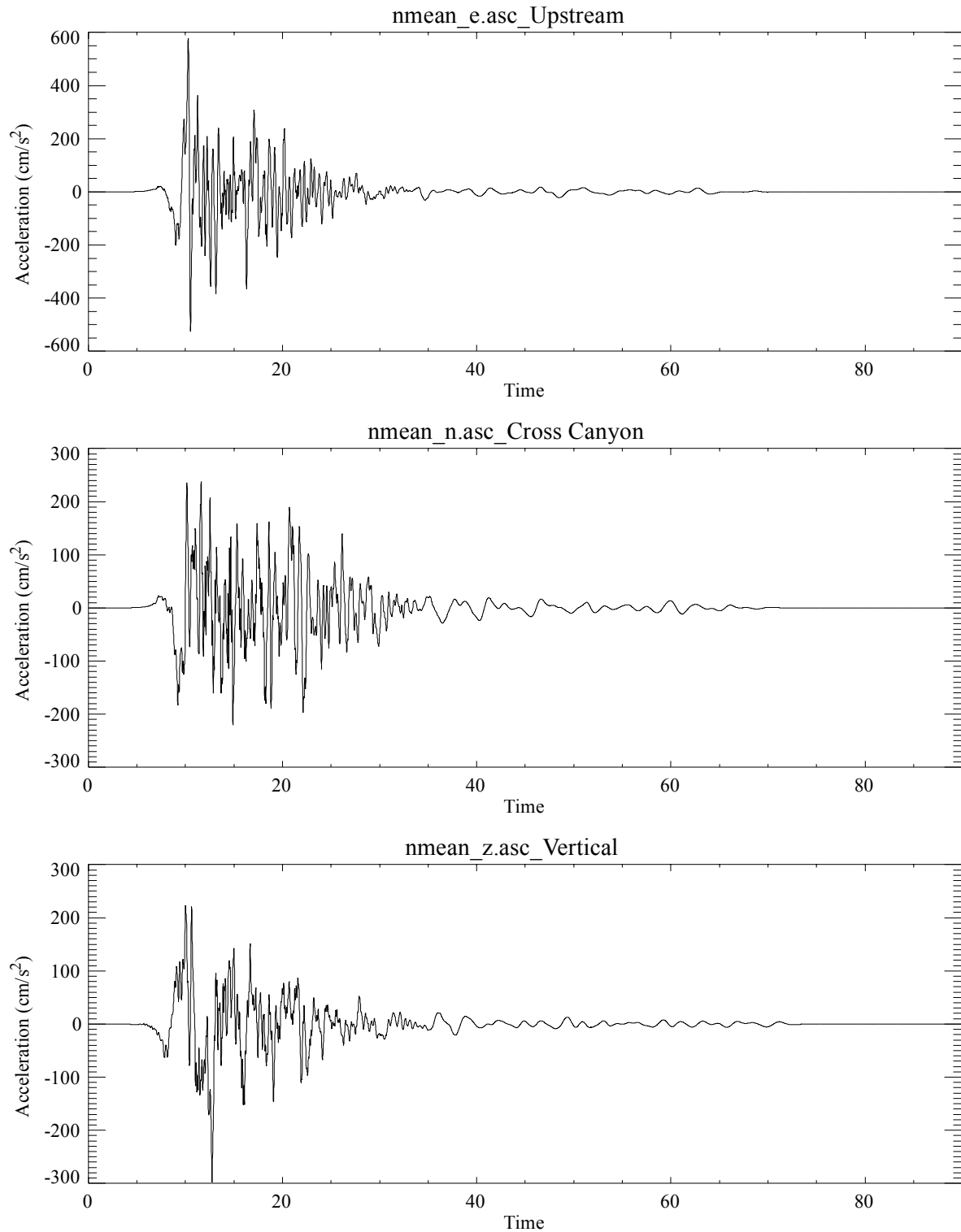
Figure 8-7: Northern Teton fault segment mean rock synthetic ground motion acceleration time histories.   Components are as labeled.

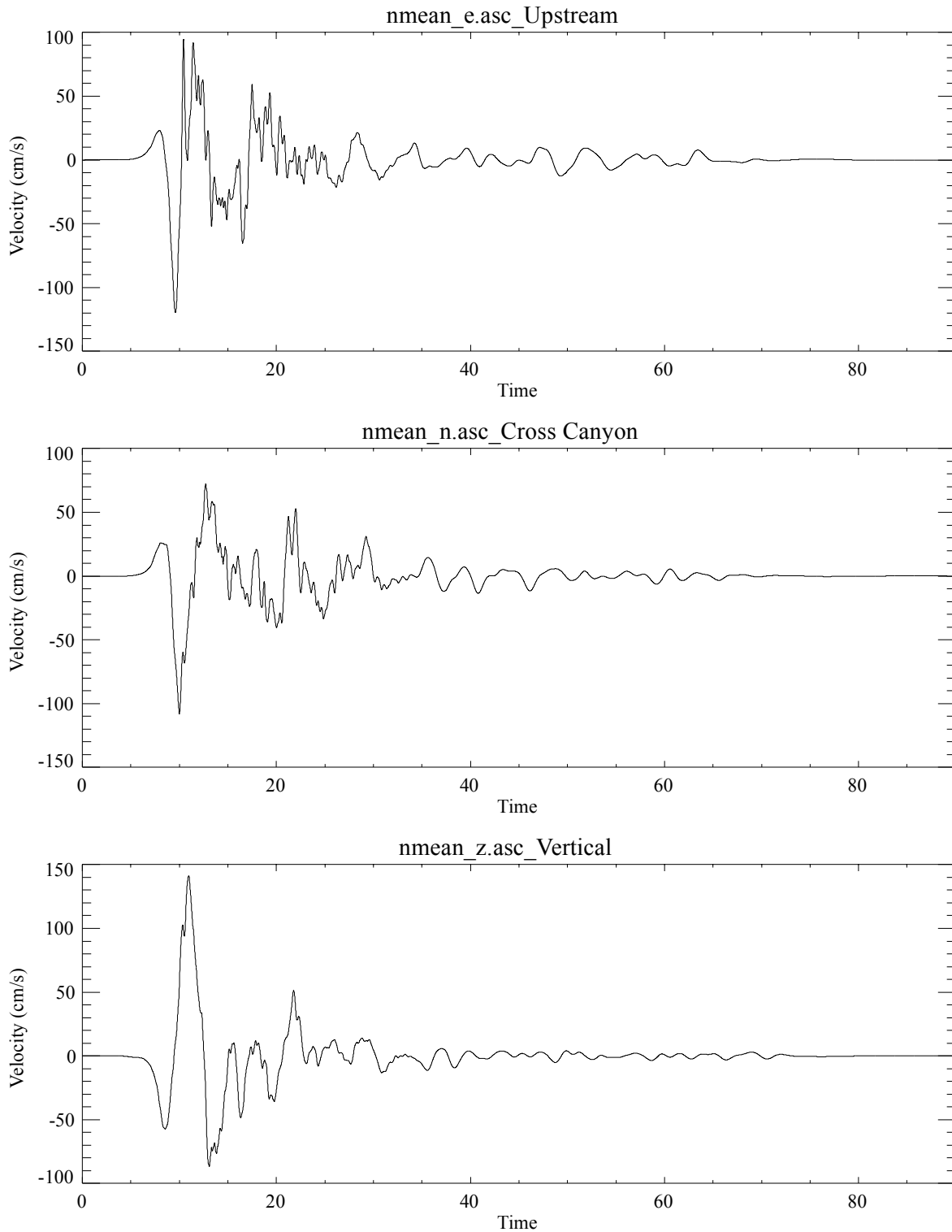Figure 8-8: Northern Teton fault segment mean rock synthetic ground motion velocity time histories. Components are as labeled.
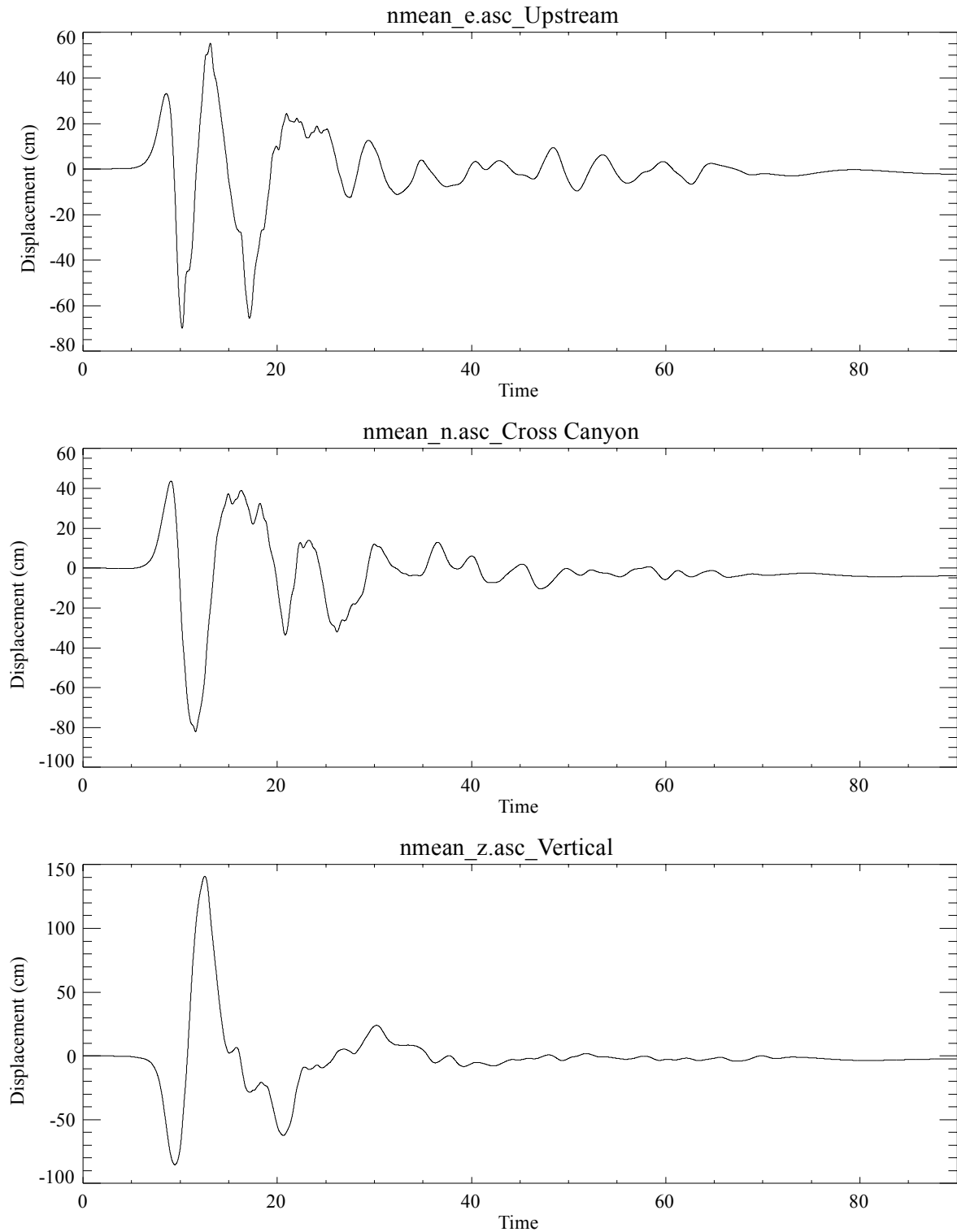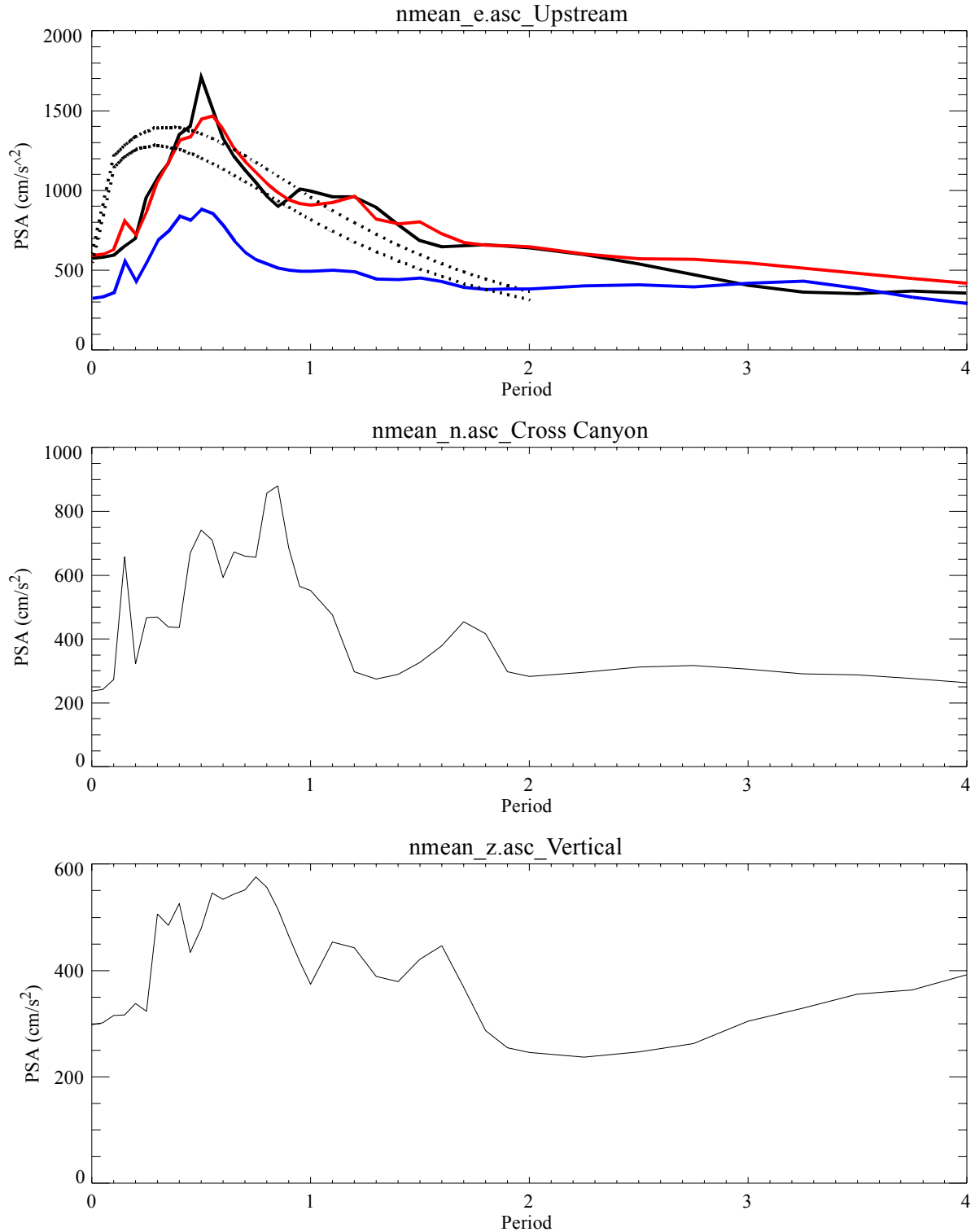
nmean_e.asc_Upstream

nmean_n.asc_Cross Canyon

nmean_z.asc_Vertical

Figure 8-9: Northern Teton fault segment mean rock synthetic ground motion displacement time histories.   Components are as labeled.

Figure 8-10: Northern Teton fault segment mean rock synthetic ground motion acceleration response spectra.   Components are as labeled. Red curve is the mean 35° dip result and the blue curve is the 60° dip result. Upper dotted curve is the Spudich et al. (1999) soil estimate for the 35° dip fault and the lower dotted curve is the empirical soil estimate for the 60° dip fault.
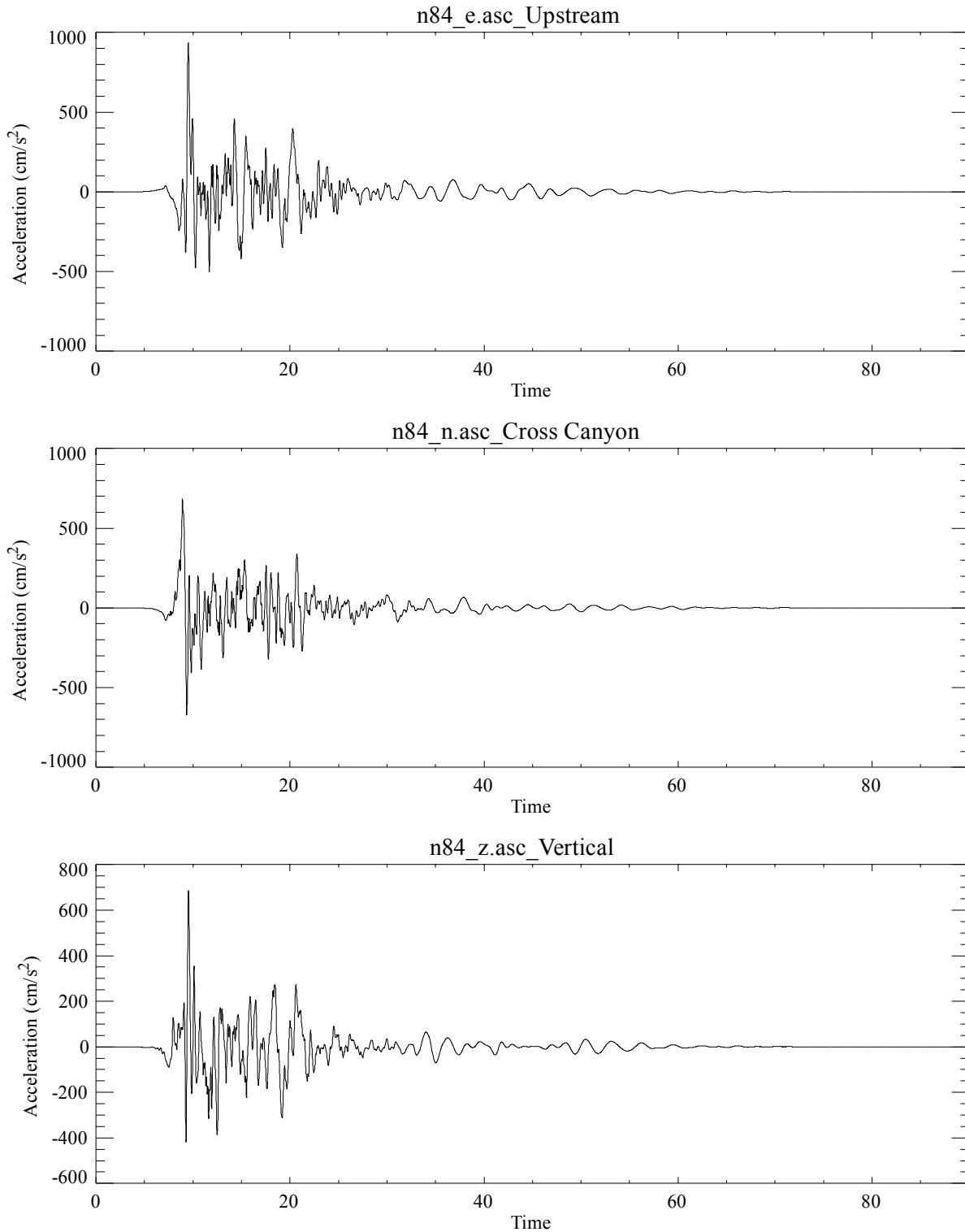
Figure 8-11: Northern Teton fault segment 84% quantile rock synthetic ground motion acceleration time histories. Components are as labeled.
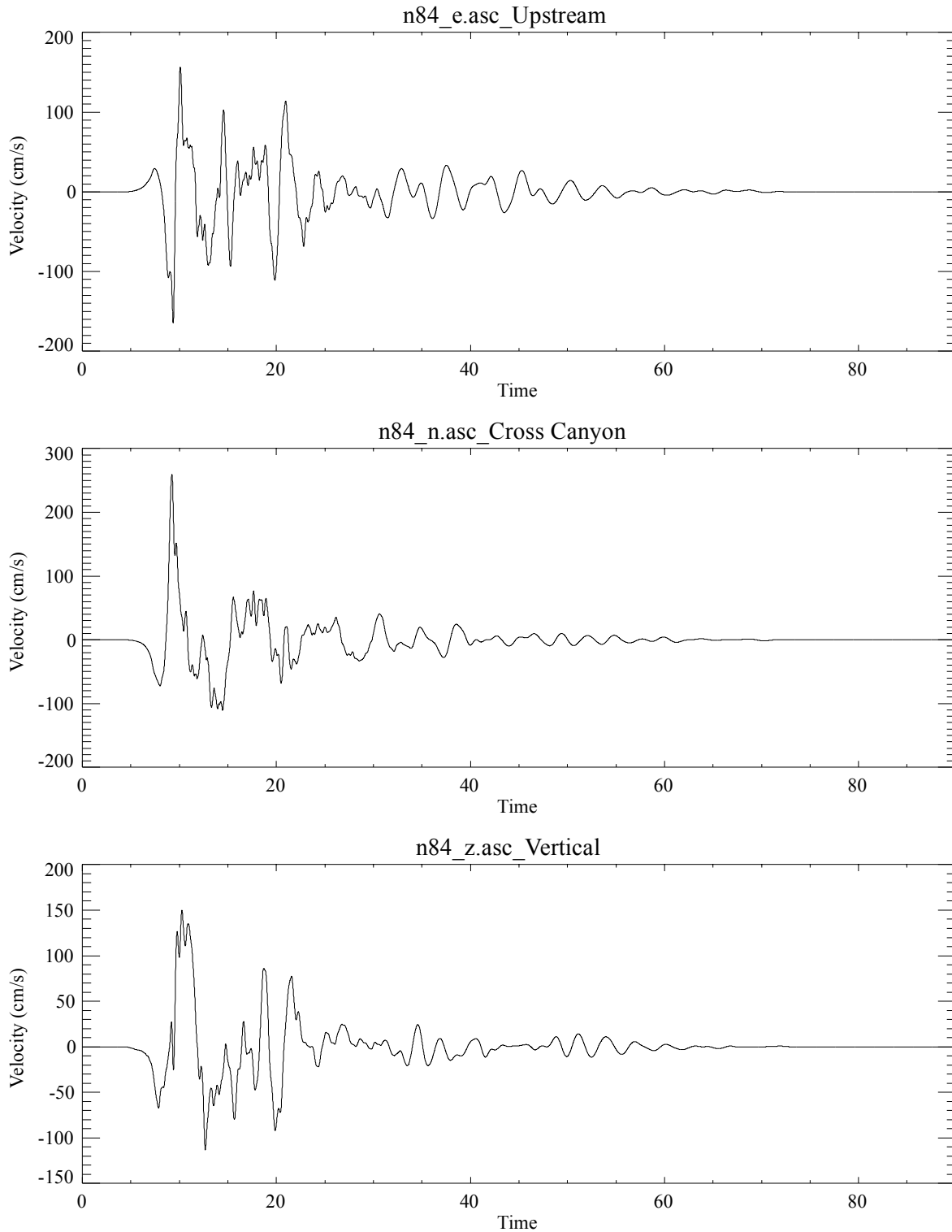
Figure 8-12: Northern Teton fault segment 84% quantile rock synthetic ground motion velocity time histories.   Components are as labeled.

n84_e.asc_Upstream

n84_n.asc_Cross Canyon
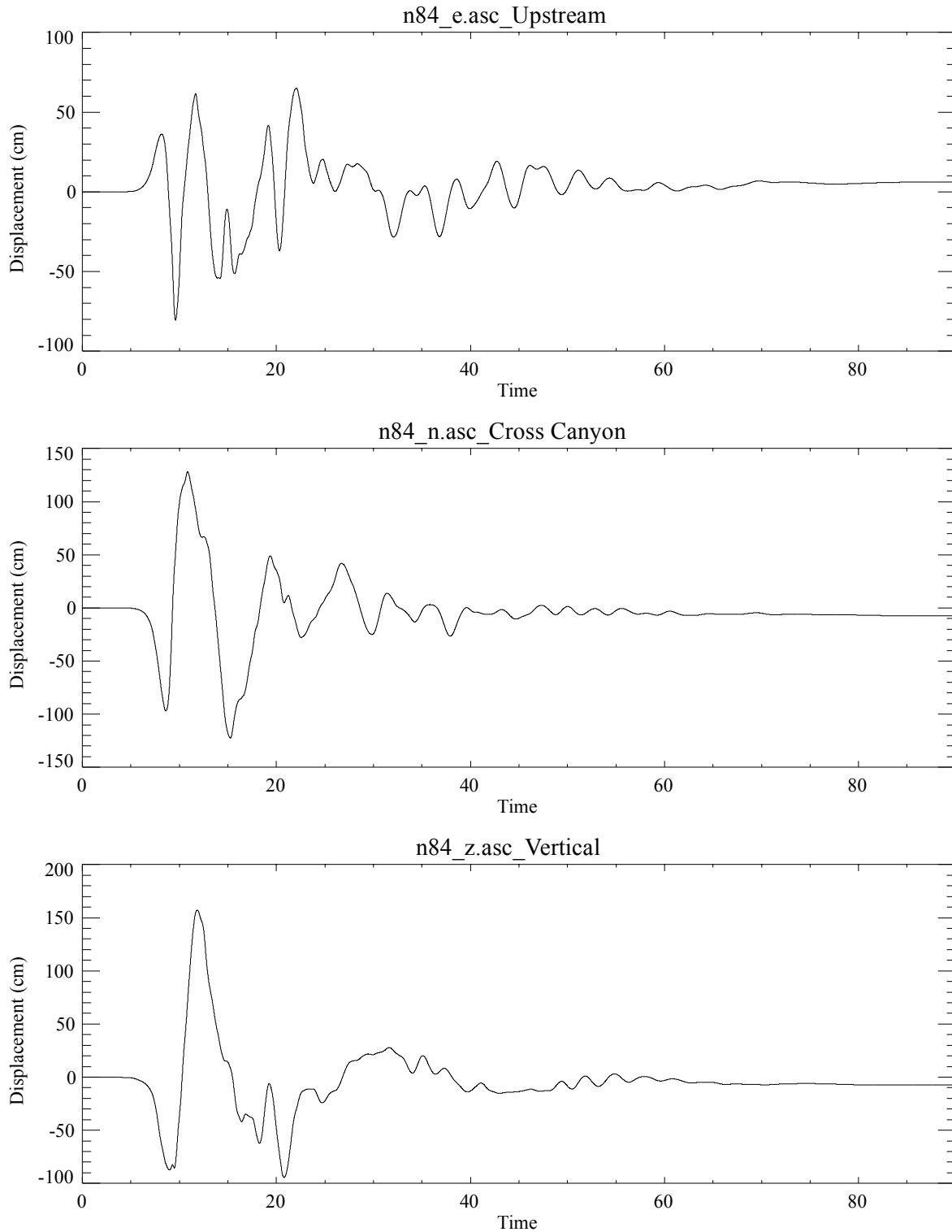

n84_z.asc_Vertical

Figure 8-13: Northern Teton fault segment 84% quantile rock synthetic ground motion displacement time histories.   Components are as labeled.
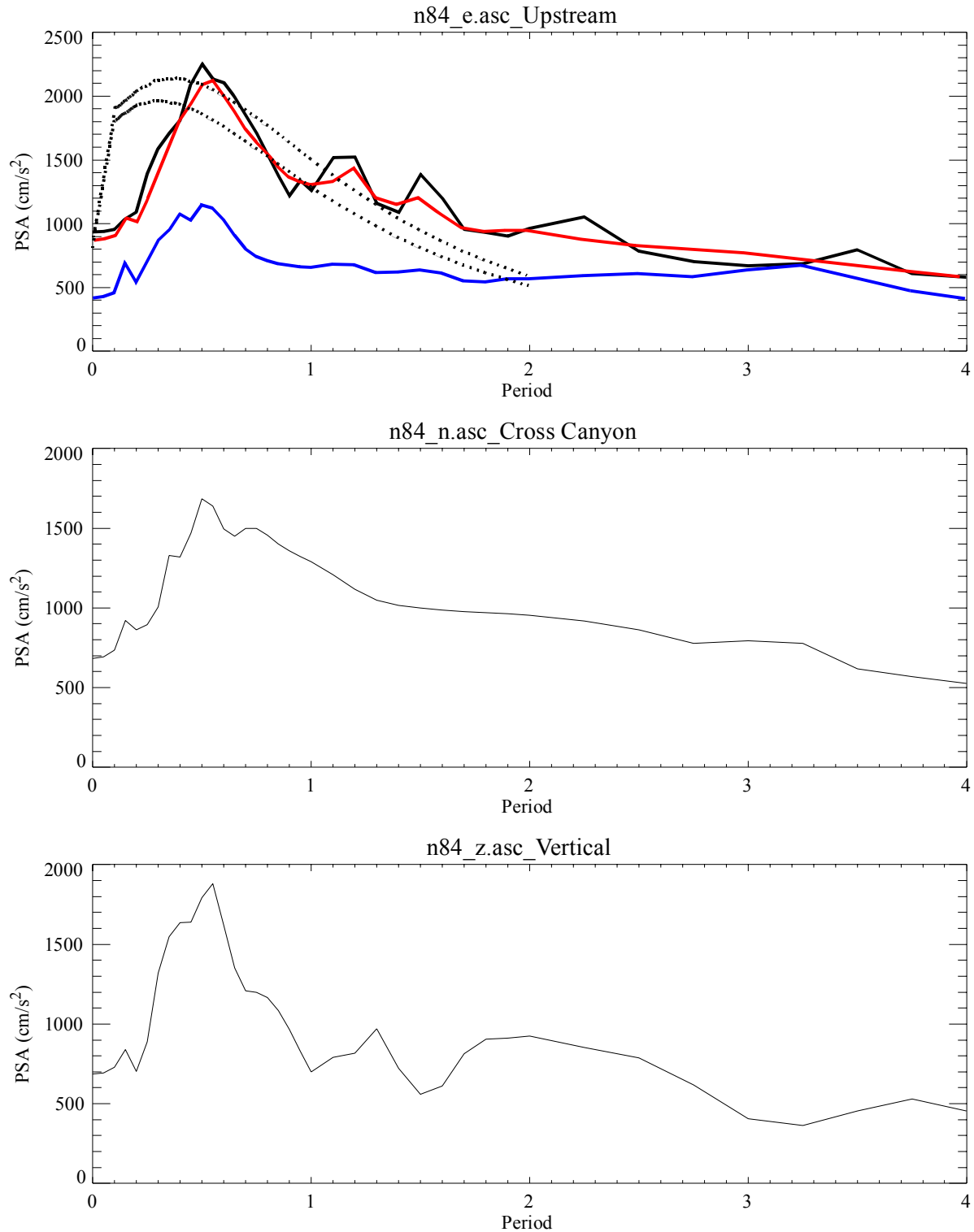
Figure 8-14: Northern Teton fault segment 84% quantile rock synthetic ground motion acceleration response spectra.   Components are as labeled. Red curve is the mean 35° dip result and the blue curve is the 60° dip result. Upper dotted curve is the Spudich et al. (1999) soil estimate for the 35° dip fault and the lower dotted curve is the empirical soil estimate for the 60° dip fault.
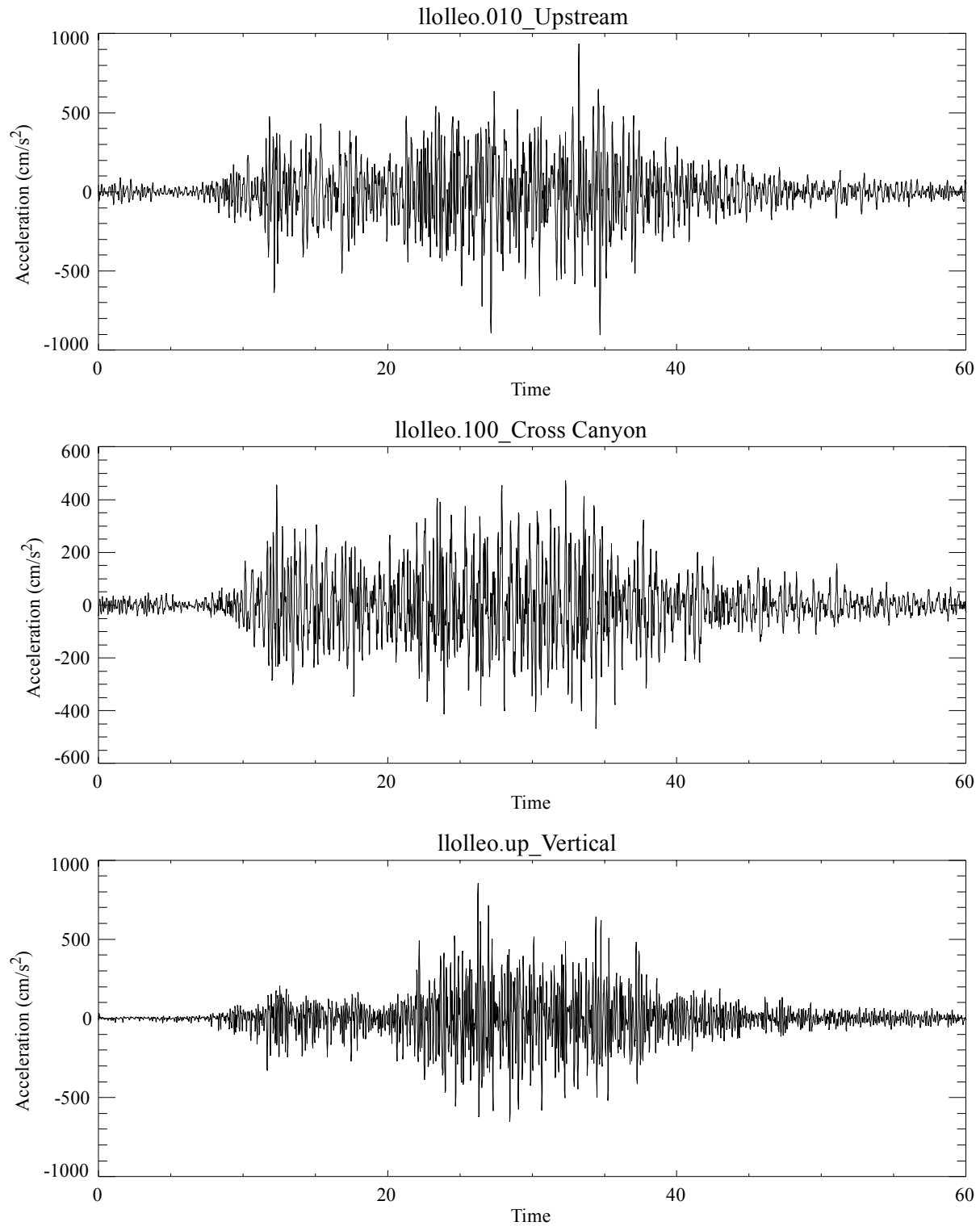
Figure 8-15: Llelleo Valparaiso, Chile, proxy for a Northern Teton fault segment rock ground motion acceleration time histories. Components are as labeled.
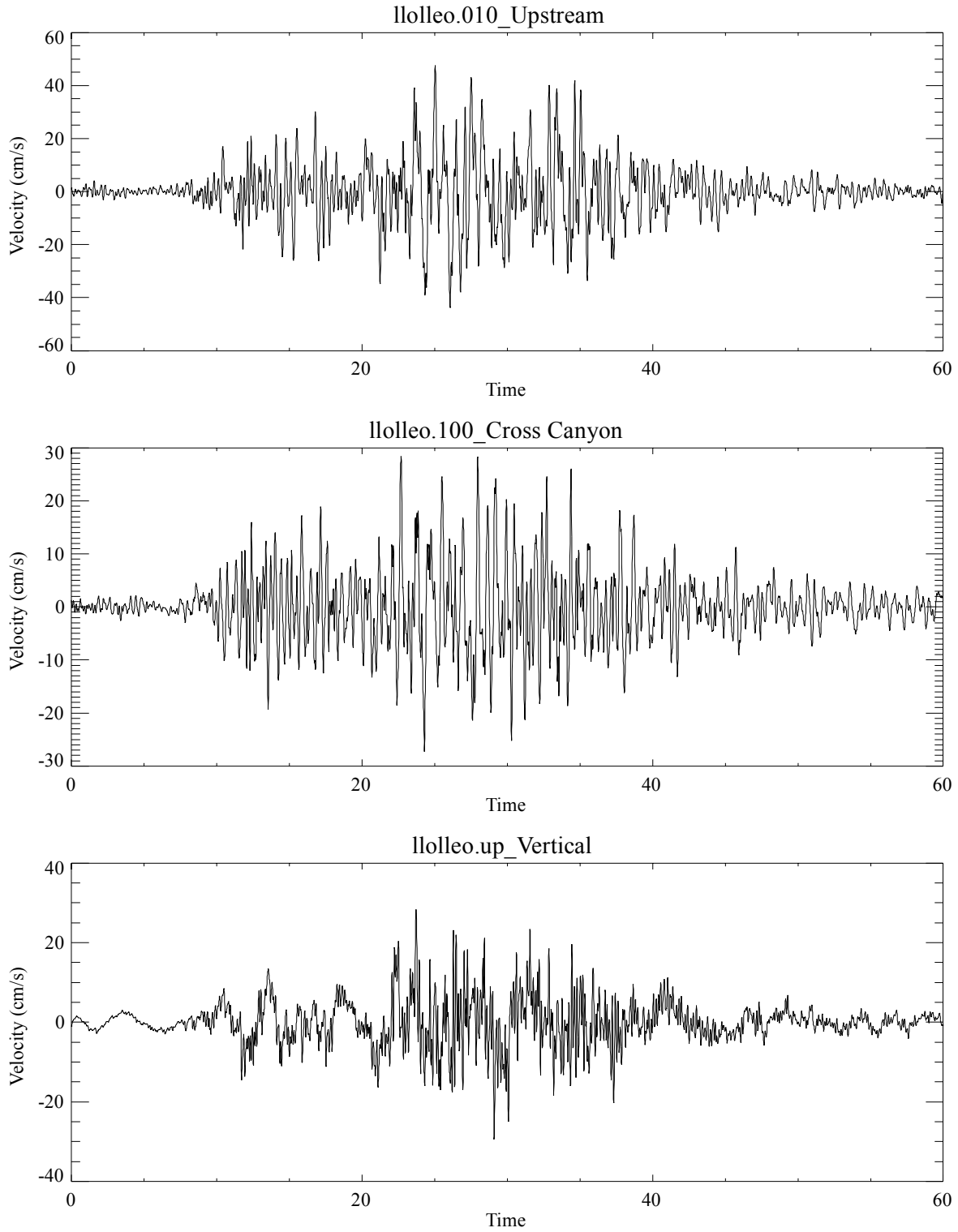
llolleo.010_Upstream

llolleo.100_Cross Canyon

llolleo.up_Vertical

Figure 8-16: Llelleo Valparaiso, Chile, proxy for a Northern Teton fault segment rock ground motion velocity time histories.   Components are as labeled.
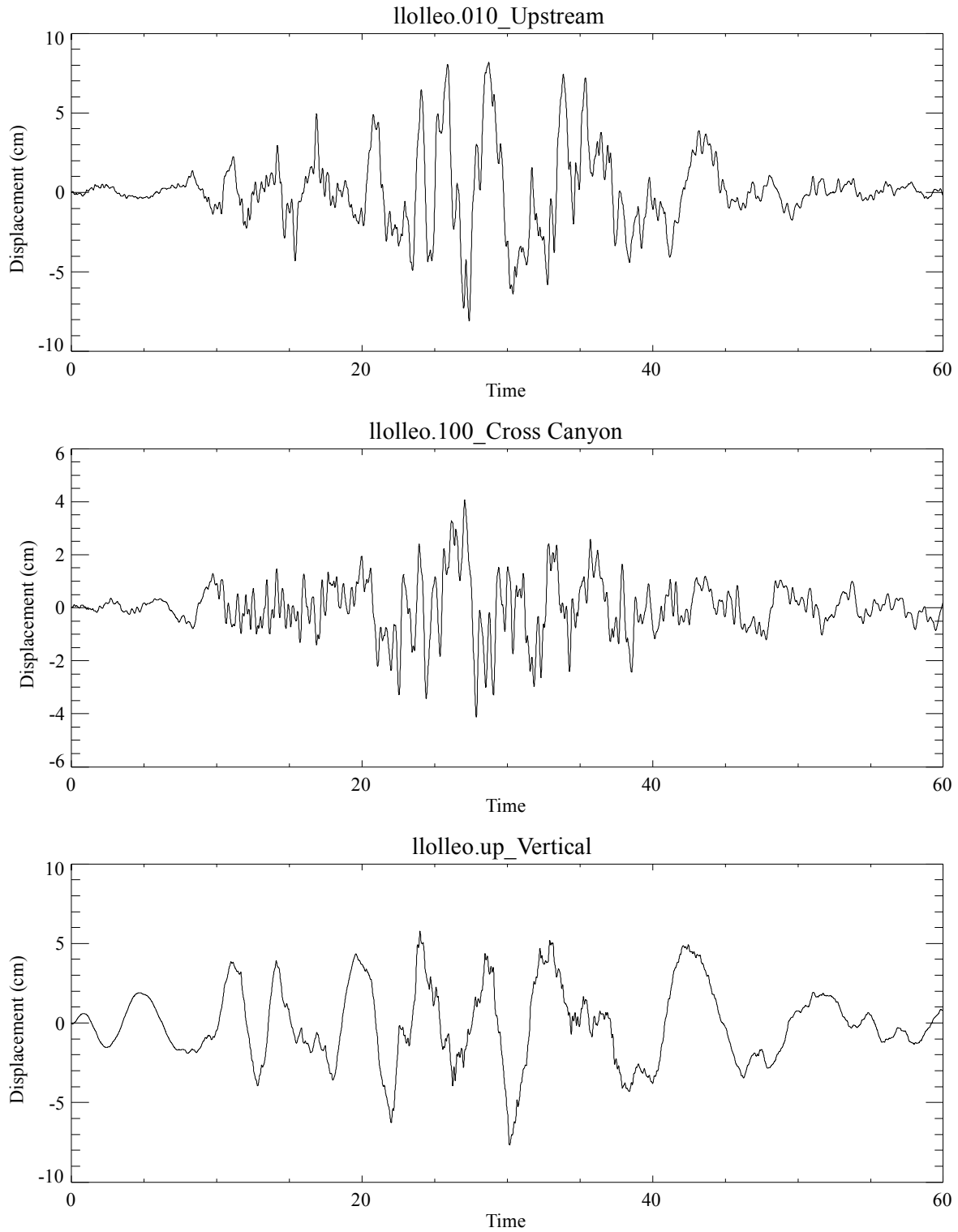
Figure 8-17: Llelleo Valparaiso, Chile, proxy for a Northern Teton fault segment rock ground motion displacement time histories.   Components are as labeled.

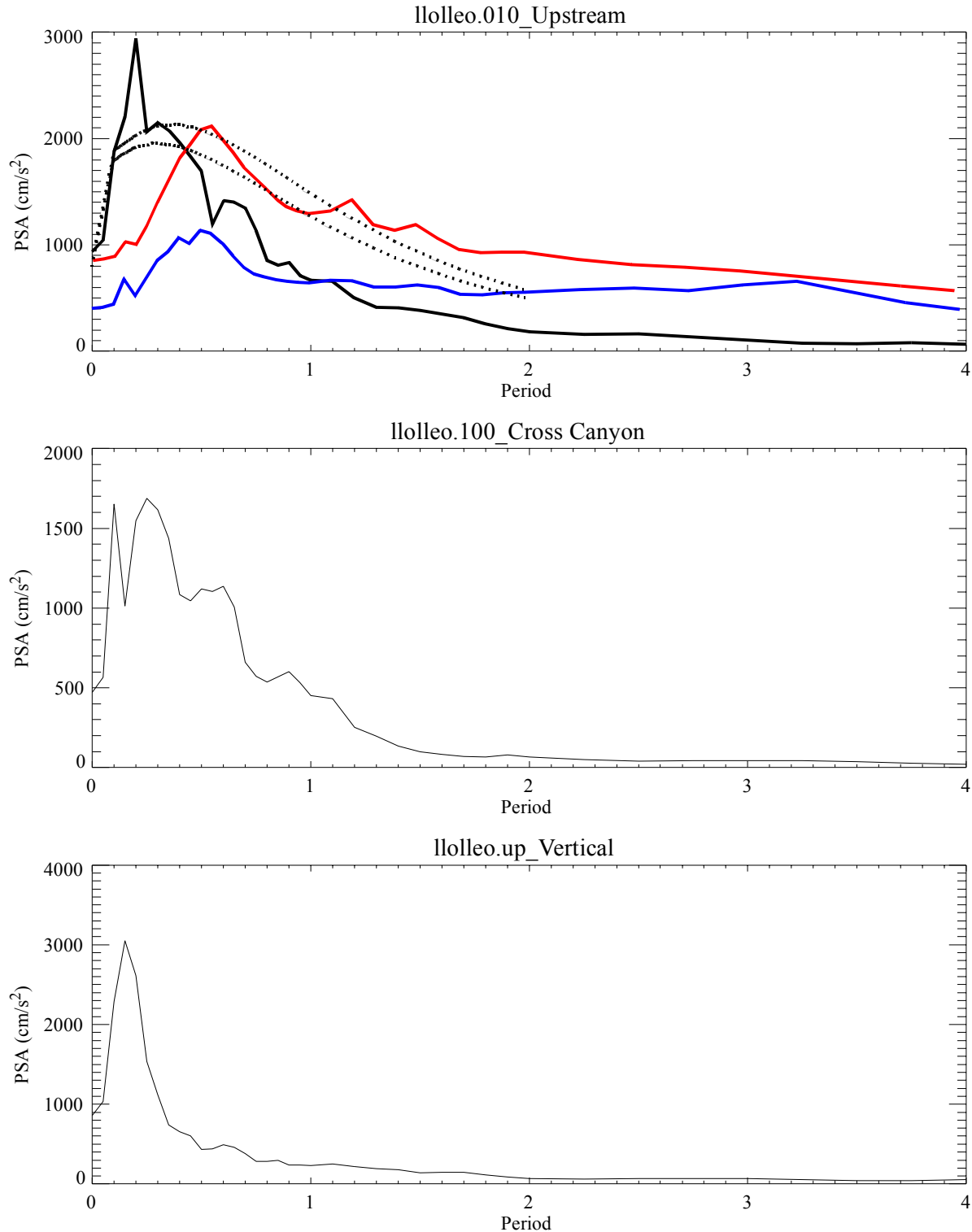Figure 8-18: Llelleo Valparaiso, Chile, proxy for a Northern Teton fault segment rock ground motion acceleration response spectra. Components are as labeled. Red curve is the mean 35° dip result and the blue curve is the 60° dip result. Upper dotted curve is the Spudich et al. (1999) soil estimate for the 35° dip fault and the lower dotted curve is the empirical soil estimate for the 60° dip fault.

earthquakes on the northern segment of the Teton fault is ~1180 years. Estimated return periods and probability weights for the ground motion time histories are provided in Table 8-6.

Table 8-6: Ground Motion Time History Annual Exceedence Probabilities

Annual probability	Lower AEP (weight = 0.25) (1/yr)	Median AEP (weight = 0.5) (1/yr)	Upper AEP (weight = 0.22) (1/yr)
Mean synthetic (Figures 8-7 to 8-10)	1/4625	1/2950	1/2000
84% quantile (Figures 8-11 to 8-14)	1/11,560	1/7375	1/5000
Lleleo (Figures 8-15 to 8-18)*	N/A	N/A	N/A
*(after record is filtered to reduce high-frequency response)			

The Lleleo record in Table 8-6 is shaded indicated that this record is only intended for sensitivity analyses.

A fourth ground motion from Section 7 that produced using the JLDW EGF's from the **M** 5.2 Idaho, earthquake, is also recommended for dynamic analyses of the concrete section of the dam . Figures 7-35, 7-37, and 7-39 may be the only available ground motion that provides realistic durations and long-period amplitudes for dynamic analyses of the dam. The caveats are that due to a lack of reference broadband recordings outside the low-velocity basin, the appropriate scaling of the amplitudes is not known and the motions may contain overamplified surface wave components. The broadband EGF synthetic motions provide more realistic amplitude and durations responses than the Lleleo record.

8.8 Recommended Acceleration Seismograms for Nonlinear Soil Analyses

Weak-motion site response was measured at Jackson Lake Dam using an array of seven broad-band seismometers. Key observations are the presence of substantial long-period amplification and prolonged duration of shaking beyond some transition point located between stations 13+00 and 24+00; minimal long-period amplification at stations 12+00 and less, referenced to a bedrock site on the right abutment; and, high-frequency de-amplification on treated sections of the north embankment referenced to a site just outside of the treated zone.

Strong ground motions at stations 13+00 and greater are expected to behave non-linearly. The observed weak-motion site response must be modified to account for non-linear soil behavior. The observed site response at station 24+00 is consistent with the 2-D and 3-D response of a sedimentary basin, and likely results from the generation of surface waves, converted phases, and interface waves. These effects are not accounted for by 1-D models. However, available computer codes for estimating non-linear soil behavior are based on propagating an incident body wave (typically a horizontally polarized S wave) through a 1-D soil column. In order to permit use of 1-D non-linear soil response computer codes, while preserving the observed 2-D and 3-D effects of prolonged duration and long-period amplification, the weak-motion impulse response is modified for input to the non-linear soil response codes at a selected reference depth. There is considerable uncertainty in this method because the reduction of the convolved surface motions to a reference depth cannot accurately account for the depth dependency of surface waves and converted phases.

The observed site responses between the rock south abutment and the deep soil portion of the embankment portion of the dam were combined with geophysical information linear 2D finite-difference modeling and nonlinear 1D modeling to estimate horizontal acceleration time histories at 140 m depth. The objective was to produce representative soil ground motion scenarios and provide acceleration time histories at ~140 m depth for use in 1D nonlinear analyses of the soil foundation. Three scenarios were used to construct ground motions for use in nonlinear soil calculations to bracket the ranges of possible ground motion inputs into nonlinear soils (Table 6-5). The most likely case is a scenario where the rock responses were convolved with JLD3 responses to obtain reasonable soil durations. However, the appropriate scaling of the resulting responses is uncertain. Consequently, two scaling scenarios with the JLD3 responses in Section 6 are recommended to facilitate sensitivity testing for nonlinear soil analyses. Table 8-6 provides probabilities to associate with the mean and 84% quantile ground motions. Probabilities were not assigned to the Tabas record, which has peak velocities comparable to the mean record and peak accelerations comparable to the 84% record and is provided for sensitivity testing between the mean and 84% ground motions.

Nonlinear effective-stress soil response calculations with NOAH show that near-surface Arias Intensities and peak acceleration responses, and their associated durations are very sensitive to input motion peak amplitudes and durations. Certain combinations of input motions produced nonlinear soil Arias Intensity and Arias duration responses that exceeded corresponding rock responses by a factor of six. Nonlinear soil response (modulus reduction) may increase ground motions durations because interface phase velocities will be reduced, increasing the time required for Airy phases to propagate from the boundaries of the glacial scour to the dam.

Probably the best way to specify input motions of dynamic analyses of the embankment section of the dam is to limit engineering foundation models to a maximum depth of 30 m with no significant impedance contrasts within the foundation material. Then, use simulated JLD3 motions produced using broadband EGF's, scaled by 0.5-0.6 as input at 30 m depth in the nonlinear engineering model. This is necessary between no 2D or even 3D FEM model of the foundation will include the 3D reverberation amplitude and duration responses using the JLDW motions as inputs. The JLD3 synthetic motions produced using the **M** 5.2 Idaho earthquake EGF's provide the only available ground motion scenario (Figures 7-53, 7-55, 7-57) for the embankment section of the dam. However, it is imperative to also use a ground motion scenario that includes the double resonance responses produced by energy arriving from north of the dam. The JLD3 synthetic motions from the **M** 4.6 Yellowstone EGF's are likely corrupted by significant whole-path surface wave responses and without an broadband recordings outside the basin there is no quantitative basis to adjust the synthetic motions. The **M** 3.2 20 Nov. 2002 earthquake is close enough to the Teton fault that there are surface waves are appropriately scaled. Unfortunately station JLD3 was no longer operating when this earthquake was recorded at JLDW. Consequently, there are no empirical soil records available to represent the duration of expected ground shaking and parasitic double basin 1-2 s amplified acceleration responses along the embankment section of Jackson Lake Dam for seismic energy incident from the north. The regional earthquake EGF's ground motion results suggest that JLD3 responses are starting to approach durations of **M** ~9 subduction zone earthquakes.

8.9 Appropriate Use of Ground Motions

Earthquake magnitude is sometimes used as a proxy for ground motion duration in engineering analyses of soils. The earthquake magnitudes used to simulate ground motions at Jackson Lake Dam from earthquakes on the Teton fault should *not* be used for this purpose. Due to the proximity of the Teton fault to the LVB and glacial scour very-low-velocity basin, and the resulting peak ground motion amplifications, extended durations, and increased Arias Intensities of ground motions at the dam, effective magnitudes for geotechnical analyses of the seismic loads are 7 1/2-8 for the rock ground motions, and are 8-9 for the soil ground motions. These recommended magnitudes for soil analyses are 0.25-0.75 to 0.5-1.5 magnitude units larger than the moment magnitudes of all-segment and northern segment rupture scenarios of the Teton fault, specifically to account for the extended durations and amplifications of ground motions observed at the dam (Sections 5 and 7). The most likely scenarios for soil response based on Sections 5 and 7 and nonlinear soil calculations using NOAH indicate ground motion durations of at least 80 seconds and possibly as long as 180 s for the embankment portion of the dam.

Jackson Lake Dam is > 1.5 km long and spans a wide variety of foundation materials with widely varying S-wave velocities and straddles a region with > 10:1 S-wave velocity contrasts. These large velocity contrasts occur between the overcompacted till (Vs ~ 1 km/s) and the soils in the glacial scour (Vs ~ 0.1 km/s). S-wave velocities also vary both laterally and vertically within the glacial scour region that is composed of fluvial-lacustrine deposits with Vs varying from to 0.09 km/s to 0.2 km/s (Sirles, 1986). Ground motions are likely to vary substantially, both along the dam's axis and in the upstream-downstream direction, because the low soil S-wave velocities result in wavelengths nearly equal to the dam's width at 1 Hz. Chen and Harichandran (2001) showed that spatially varying ground motions are likely to substantially increase shear stresses in foundation materials at the toes of an embankment dam, particularly when spatial coherence is significantly < 1 for low frequencies. Santa-Cruz et al. (1999) showed that for low-velocity basins, the absolute value of coherency can be substantially less than 1 for frequencies as low as 0.3 Hz, for separation distances as low as 800 m, and for frequencies as low as 1 Hz, for separation distances as low as 100 m. Given the results of Santa-Cruz et al. (1999), and the substantial and variable thickness of low S-wave velocity materials in the glacial scour that comprises the foundation for the embankment section of the dam, and the strongly varying site

responses noted in Chapter 5 from the Jackson Lake Dam site response stations, it is likely that ground motions coherency will be substantially < 1 for frequencies as low as 0.3 Hz along the embankment portion of the dam. Estimated differential displacements between the concrete section and the soil section are likely to exceed 50 cm both along the dam's axis and in downstream shear, although the length scale over which the differential displacements will occur is unknown.

The southern portion of the dam, consisting primarily of the concrete section, is founded on ~1 km/s S-wave velocity till and tuff. The rest of the dam is founded on ~0.1 km/s S-wave fluvial-lacustrine deposits that increase in thickness towards the northern end of the dam. The southern portion of the dam will shake less strongly and for shorter durations than the rest of the dam. Consequently, the largest strains resulting from differential motions along the axis of the dam are likely to be located in the embankment section extending from the concrete section to station 32, where Sirles (1986) found a ~140 m thick section of fluvial-lacustrine deposits below the ground surface. The distances between stations JLD2 near the northern end of the concrete section and station JLD3 near station 24+00 is 356 m. For a vertically-incident shear wave, the propagation delay at station JLD3 relative to JLD2 due to ~140 m of fluvial-lacustrine fill with an average S-wave velocity of ~140 m/s is 0.87 s (1 s travel-time through the last 140 m for JLD3 and 0.13 s travel time through the last 140 m for JLD2). This yields a S-wave apparent velocity of 0.41 km/s, which will likely reduce S-wave coherency at low frequencies, based on the results of Santa-Cruz et al. (1999). This is an apparent velocity 10 times *smaller* than considered by Chen and Harichandran (2001) in their analyses of the influence of coherency on the dynamic analysis of embankment dams. Since the peak velocity loads at Jackson Lake Dam are substantially larger than considered by Chen and Harichandran (2001), and apparent velocities are much lower, differential displacements, and correspond strains and stresses are likely to be larger at Jackson Lake Dam than those considered in Chen and Harichandran (2001). S-wave apparent velocities will decrease for S-waves arriving from the south (about half of the northern Teton rupture segment, and the entire southern Teton rupture segment). S-wave apparent velocities will be increased slightly for S-wave arrivals from north of station JLD3, but the increases in apparent velocity will be modest.

Uncertainties about the velocity structure and spatial extent of the glacial scour produce uncertainties of about a factor of two in peak soil ground motions, and factor of four uncertainties in soil ground motion durations. It is necessary to determine the wave-types that comprise the long duration soil ground motions to determine the appropriate methods to calculate nonlinear soil responses. Synthetic calculations in Section 5 indicate that a significant fraction of the long-duration high-amplitude soil motions at the dam may be produced by S-waves and horizontally propagating interface waves occurring at depth in the glacial scour basin.

Consistent with past approaches to reduce ground motion estimation biases and uncertainties (Anderson and O'Connell, 1998; Anderson and O'Connell, 1993; O'Connell and Unruh, 2000; Ake et al., 2002) microearthquake data from the Jackson Lake Seismic Network provided the crucial information about the subsurface fault geometries, particularly dip of faults at depth, and seismotectonic constraints on state-of-stress and fault kinematics, information necessary to estimation ground motions at Jackson Lake Dam. The combination of broadband site response stations at Jackson Lake Dam and the short-period JLSN provided empirical Green's functions and the ability to estimate site responses in the same manner as the site response stations in previous studies (O'Connell and Ake, 1995; O'Connell, 1999b; O'Connell and Unruh, 2000; O'Connell, 2001), where local seismographic networks such as the short-period Southern California Seismic Network and the Northern California Seismic Network provided crucial information necessary to convert site response recordings into empirical Green's functions. The development of site-specific ground motions using empirical Green's functions substantially reduced ground motion biases in several previous studies (O'Connell, 1999a, 1999b; O'Connell and Unruh, 2000; O'Connell, 2001). For instance, site-response recordings used in conjunction with short-period data from the Southern California Seismic Network showed that convention approaches to estimating near-source ground motions at stiff-soil sites in southern California were likely to strongly overpredict peak ground motions (O'Connell, 1999a). At a high-velocity hard-rock site, broadband site-response data in conjunction with short-period data from the Northern California Seismic Network showed that source characterization of blind thrust faults in the western Sacramento Valley were incorrect (O'Connell and Unruh, 2000; O'Connell et al., 2001) and that peak acceleration loads would likely be about 2/3 empirical predictions, resulting in substantially lower final peak ground motion estimates (LaForge, 1999). Estimation of the 3D

velocity structure of the crust and discovery of the significant impacts of 3D velocity structure on peak ground motions and ground motion durations were made possible by the earthquake data from the JLSN and the broadband site response seismographs at Jackson Lake Dam. The earthquake data provided by the JLSN were necessary to fully exploit the site response earthquake recordings to develop empirical Green's functions and site response information for nonlinear soil analyses. At Jackson Lake Dam, development of site-specific ground motions increases confidence that estimated ground motions are not likely to be significantly biased. The fact that alternative ground motion synthesis methods in Section 7 produced similar ground motion estimates, suggests that the ground motions recommended for dynamic analyses of Jackson Lake Dam are reasonable.

The stochastic characteristics of earthquake occurrence means that seismic monitoring may or may not record additional earthquakes on the Teton fault. However, in previous studies the operation of two three-component broadband instruments on the hanging wall of the Red Mountain fault in the Transverse Ranges of southern California for less than one year produced valuable data for constraining the downdip dip geometry of the Red Mountain fault (Anderson and O'Connell, 1998). Adding these two three-component stations to a predominantly short-period vertical seismographic network reduced hypocenter depth uncertainties on the Red Mountain fault to < 1 km (Anderson and O'Connell, 1998). Of particular interest, was the recording of numerous earthquakes < **M** 1.5 by these stations that went unrecorded by most of the more distant stations in the network, and thus were not included in the earthquake catalog. Near the Ortigalita fault along the western margin of the San Joaquin Valley, California, < 1 year of earthquake recordings from four broadband three-component stations located near the dams provided valuable constraints on the depth and dip of blind thrust faults below the dams that was not available from the local short-period seismographic network operated by the California Department of Water Resources.

Based on the significantly longer rock site durations at Jackson Lake Dam indicate that there must be some fundamental differences between the physical properties of the large-scale low-velocity basins at Jackson Lake and Mexico City. More importantly, at Jackson Lake Dam soil sites there appears to be a parasitic interaction of nearly-identical-period resonant responses between the soil

basin containing the embankment portion of the dam, and the large-scale low-velocity basin for periods of 1-2 s, which produces unusually long sustained peak accelerations of ~0.25 g lasting up to 70 s. The Jackson Lake Dam site responses instruments were necessary to discover the range of ground motion responses likely to occur in a such a complex geological and geophysical setting, particularly for the wide range of incidence angles and azimuths associated with seismic energy radiated by the Teton fault. The value of broadband site response recordings of small earthquakes was also demonstrated in investigations of anomalously-large peak accelerations in Santa Monica, California, in response to the 1994 **M** 6.7 Northridge earthquake (Davis et al., 2000). Davis et al. (2000) discovered a relatively small-scale crustal velocity lens that substantially amplifies ground motions for a limited range of azimuths, including azimuths associated with wave arrivals from the Northridge earthquake. It would be difficult and expensive to discover such a small velocity structure using exploration geophysics methods; the earthquake recordings were clearly the most efficient and compelling means to discover important ground motion anomalies. An importance difference between Santa Monica and Jackson Lake Dam, is that at Jackson Lake Dam, the broadband site-response recordings and local seismic network afforded the opportunity to identify significant ground motion characteristics prior to the occurrence of a large, nearby earthquake. It appears that there may be other low-velocity basins in the ISB with characteristics similar to Jackson Lake (Zoback, 1983). Studies in other low-velocity basins in the ISB would likely benefit from a combination of the approach used in the study and the approach of Davis et al. (2000), by combining broadband recordings of local and regional earthquakes from sites inside the basin and from sites located on high-velocity portions of the footwall outside the low-velocity basin, to facilitate deconvolution of the basin responses from incident seismic energy.